Bitstream Photon Counting Chirped AM Lidar with a Digital Logic Local Oscillator: Concept, Various Configurations, Theory, Simulations and Proof-of-Concept Experiment

Brian C. Redman, retired, no institutional affiliation, email: bredman@rocketmail.com

Abstract

This paper introduces the bitstream Photon Counting Chirped Amplitude Modulation (AM) Lidar (PC-CAML) with a Digital Logic Local Oscillator (DLLO) concept in various configurations.

Rather than using a radio-frequency (RF) analog local oscillator (LO) applied electronically either in post-detection mixing or via opto-electronic mixing (OEM) at the detector, or applied via pre-detection mixing using an optical intensity modulator, as in previous PC-CAML systems, the new method mixes the single-bit binary counts from the photon counting detector with a single-bit binary LO using a digital logic gate. This type of LO is called the Digital Logic Local Oscillator (DLLO), and the resulting system is called bitstream PC-CAML.

The key advantage of the DLLO is that it replaces bulky, power-hungry, and expensive wideband RF analog electronics with single-bit digital logic components that can be implemented in inexpensive silicon complementary metal-oxide-semiconductor (CMOS) read-out integrated circuits (ROICs) to make the bitstream PC-CAML with a DLLO more suitable for compact lidar-on-a-chip systems and lidar array receivers than previous PC-CAML systems.

This paper presents the DLLO for bitstream PC-CAML concept along with an initial signal-to-noise ratio (SNR) theory with comparisons to Monte Carlo simulation results and initial proof-of-concept experimental results. Using the simulation results, the improvements in SNR provided by using a bipolar DLLO and digital I/Q demodulation configuration compared to the original single channel unipolar DLLO without digital I/Q demodulation configuration, and provided by using the new concept of a dual unipolar (DU) transmitted signal to yield a bipolar signal in the receiver are demonstrated.

1. Bitstream PC-CAML with a DLLO Concept

The patented photon counting chirped amplitude modulation lidar (PC-CAML) concept has been extensively discussed previously. [ref 1-13] In previous PC-CAML systems, the local oscillator (LO) has been a radio-frequency (RF) analog signal applied using expensive, bulky, and power hungry RF analog electronics either in post-detection mixing or via opto-electronic mixing (OEM) at the photon counting detector, including gating of the detector, or applied via pre-detection mixing using an optical intensity modulator as illustrated in figure 1. [ref 1-13] The reader is referred to references 1-13 for more details on the traditional PC-CAML system.[1]

1 Note that in reference 8 from 2013, Zhang, et. al., claim that they were the first to apply the LO signal directly to the gate of the Gm-APD detector in a method that they called smart premixing. However, in reference 3 from 2006, Redman, Ruff, and Giza published results from applying the LO directly to the gate of the Gm-APD in a method they called opto-electronic mixing (OEM) to distinguish it from post-detection mixing using an RF LO after the detector, and from pre-detection mixing using an optical modulator prior to the detector. Redman, et. al., used a chirped square wave LO applied to the gate of the Gm-APD, whereas Zhang, et. al., used a pulse width modulated sampling of a chirped sinusoid for their LO applied to the gate of the Gm-APD.

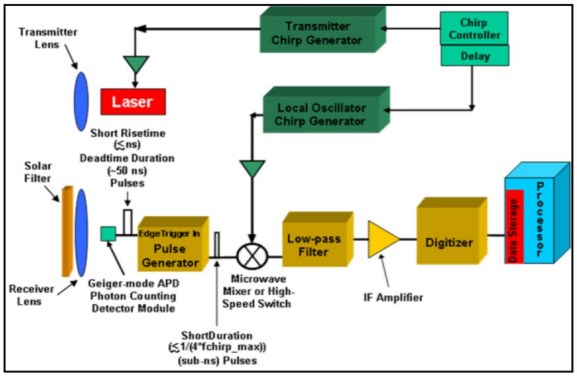

(a.)

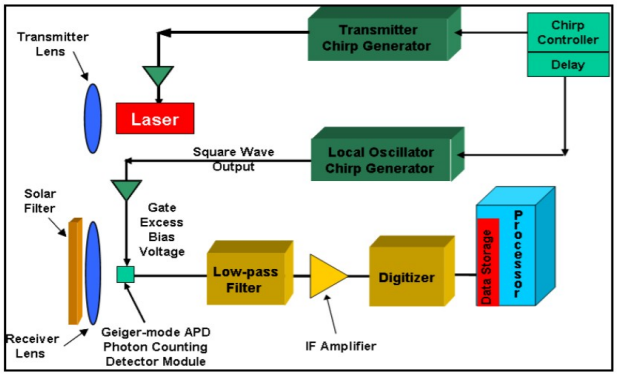

(b.)

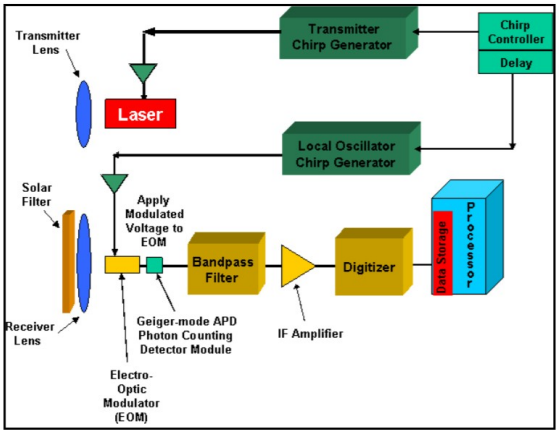

(c.)

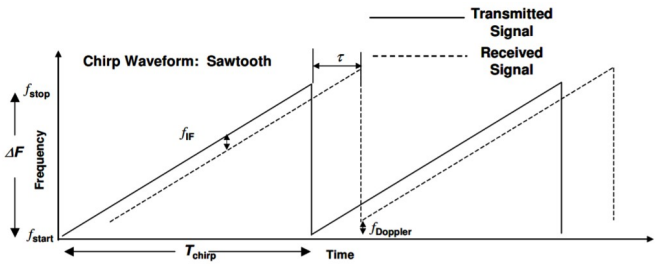

(d.)

$$f_{IF} = \tau \frac{\Delta F}{T_{chirp}} = \frac{2R\Delta F}{cT_{chirp}}$$, where f_{IF} = the target return's intermediate frequency

τ = target round-trip delay time,

$\Delta F = f_{stop} - f_{start}$ = chirp bandwidth,

T_{chirp} = chirp duration

R = target range

c = speed of light

(e.)

Figure 1. Traditional Photon Counting Chirped Amplitude Modulation Lidar (PC-CAML) Configurations and Waveforms: (a.) Post-detection Mixing Configuration, (b.) Opto-Electronic Mixing (OEM) Configuration, (c.) Predetection Mixing Configuration, (d.) Sawtooth Chirp Waveform applied to the transmitted amplitude modulation, and (e.) Equation relating the stationary target (no Doppler frequency shift) intermediate frequency (IF), f_{IF}, to the target range and chirp waveform parameters. [ref 3 and 5]

Alternatively, one can dispense with an LO in the receiver altogether by sending the wideband, high speed single-bit photon count data output from the photon counting detector directly to storage and demodulating the chirp digitally. [ref 14] However, this alternative eliminates a key advantage of the PC-CAML concept, which is the down conversion of the wide bandwidth ranging signal to the low bandwidth intermediate frequency (IF) regime where low sampling rate

analog-to-digital converters (ADCs) can be used to digitize the lidar data which is then sent to storage and digital processing at a low data rate. This down sampling to a lower data rate gains in importance as the number of detectors used increases, such as for larger format array receivers, since it is far easier and less costly to move data from the ROIC to data storage and processing for multiple parallel data streams at low data rates than at high data rates.

This paper presents and discusses a new alternative for applying the LO in the PC-CAML concept called the Digital Logic Local Oscillator (DLLO). For the simplest case of a single channel, unipolar DLLO, and unipolar signal, the constant amplitude, single-bit output count of the photon counting detector receiving a chirped AM signal is input to an edge-triggered pulse detector which outputs a very short single-bit digital logic level pulse to one input of an AND binary digital logic gate, and the other input of the AND binary digital logic gate is connected to the single-bit digital logic level binary data stream of a chirped AM LO signal, as shown in figure 2 (a.). The wideband, high speed single-bit digital data output by the AND binary digital logic gate can be either directly sent to storage and fully digitally processed, or sent through an analog or digital low/band pass filter in the IF band, the output of which is either digitized by a low sample rate analog-to-digital converter (ADC), or digitally down sampled to a low sample rate, respectively, as shown in figure 2 (a.). The low sample rate digital data is then sent to storage and digitally processed by the usual methods for chirped AM lidar. In this concept, the AND binary digital logic gate provides the mixing of the single-bit photon count data from the Geiger-mode Avalanche PhotoDiode (Gm-APD) with the single-bit LO data.

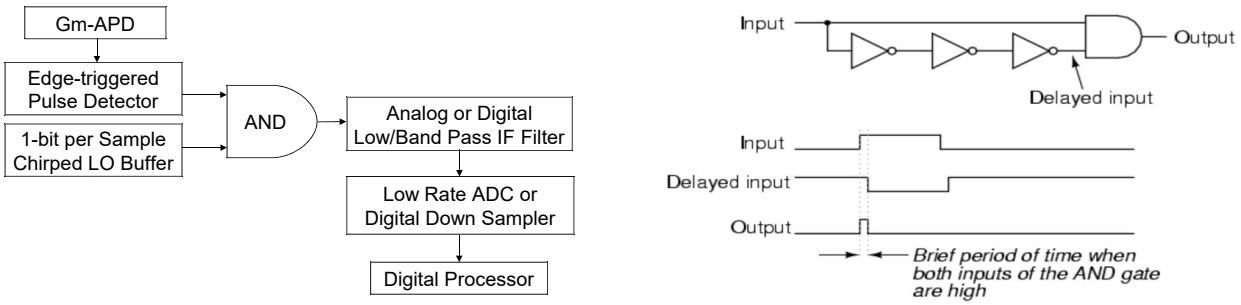

(a.) (b.)

Figure 2. (a.) DLLO for Bitstream PC-CAML Concept Diagram and (b.) Example Edge-triggered Pulse Detector circuit from the online textbook Lessons in Electric Circuits, at https://www.allaboutcircuits.com/textbook/digital/chpt-10/edge-triggered-latches-flip-flops/ , by Tony R. Kuphaldt and Dennis Crunkilton, License: https://www.gnu.org/licenses/dsl.html .

An example circuit for the edge-triggered pulse detector is shown in figure 2 (b.). The edge-triggered pulse detector allows the count pulses input to the AND gate to be much shorter than the count pulses output by the Gm-APD, which can be longer than desired due to the Gm-APD dead-time. The edge-triggered pulse detector's output pulse can be as short as a single clock pulse as long as the rising edge of the Gm-APD's count pulse is shorter than a clock pulse, and the delay on the delayed input in the edge-triggered pulse detector circuit is shorter than a clock pulse. Other types of edge-triggered pulse circuits may be used, or the edge-triggered pulse circuit can be eliminated if the Gm-APD count pulses are short enough.

The concept of a DLLO has not been previously applied to lidar, but it was recently introduced for radar and called bitstream or single-bit radar. [ref 15-18] There are two articles from 2014 that used the term bitstream for a random pulse modulation photon counting ranging system. [ref 19-20] Therefore, the PC-CAML with a DLLO is referred to as the bitstream PC-CAML. The use of a DLLO in the bitstream PC-CAML is a novel technique for bitstream lidar since the random bitstream ranging system described in the references 19 and 20 does not involve the use of a local oscillator.

1.1 Key Advantages of the DLLO in Bitstream PC-CAML

The key advantages of the DLLO in the bitstream PC-CAML are as follows:

1. The DLLO can be implemented in the unit cells of a photon counting lidar receiver's readout integrated circuit (ROIC) by adding binary digital logic gates.
2. The signal and LO count data consist of just streams of digital data.
3. The DLLO eliminates the need for bulky, power-hungry, and expensive wideband RF analog receiver electronics by replacing them with digital logic receiver electronics. Multi-GHz clocks and digital logic gates are readily implemented in inexpensive silicon complementary metal-oxide-semiconductor (CMOS) ROICs.
4. The DLLO single-bit binary waveform data can be computed prior to operation and stored in a buffer in each ROIC unit cell, or in a single buffer in the receiver and distributed to each ROIC unit cell in real-time during operation. The buffer can be a circular buffer for continuous repetition of the DLLO waveform.

These advantages make the bitstream PC-CAML with a DLLO more suitable for compact lidar-on-a-chip systems and lidar array receivers than previous PC-CAML systems.

1.2 Differences Between Bitstream PC-CAML and Bitstream Radar

The main differences between the bitstream PC-CAML and the bitstream radar are

1. In the simplest case, the bitstream PC-CAML's signal and LO are unipolar, whereas the bitstream radar's signal and LO are bipolar, which makes the appropriate binary digital logic gate an AND gate for the former and an XOR gate for the latter [ref 18, pp. Iii, 8, 117]. Extensions of the bitstream PC-CAML for a bipolar LO and a dual unipolar (DU) transmitted signal are discussed later in this paper.
2. The photon counting detector output in PC-CAML is inherently a single-bit binary data stream even when the transmitted signal is analog, whereas the bitstream radar needs to use thresholds, comparators, and/or limiters to convert the transmitted or received signal to a single-bit binary data stream [ref 18, pp. 6-10, 13, 36-40].
3. The bitstream radar needs dithering on the transmitter or an analog low pass anti-aliasing filter and multi-bit ADC on the receiver to avoid aliasing [ref 18, p. 56], but the bitstream PC-CAML does not need either when the receiver is operating well below saturation due to the alias-free random sampling provided by the received photon counts.

1.3 Unipolar vs. Bipolar Local Oscillator and Signal

Using a bipolar local oscillator (LO) and/or a bipolar signal provides better SNR compared to that when using a unipolar LO and/or a unipolar signal. However, the simplest implementation of the PC-CAML shown in figure 2 (a.) is one in which the DLLO and the signal are both unipolar. The implementation with a bipolar DLLO is described in section 1.3.2.

It was previously thought that the chirped AM signal could only be unipolar since the light power or intensity is being modulated and the power/intensity cannot be negative. The novel technique of using a dual unipolar (DU) chirped AM transmitted signal to provide a bipolar signal in the receiver is described in section 1.3.4.

1.3.1 Unipolar Signal and Unipolar DLLO

The unipolar nature of the PC-CAML signal and DLLO in the simplest implementation shown in figure 2 (a.) makes the AND digital logic gate the appropriate replacement for the analog mixer for the bitstream PC-CAML in this case instead of the XOR (Exclusive OR) digital logic gate used for the bitstream radar [ref 15-18] since the Boolean logic truth table for the AND Boolean operator corresponds to multiplication for 0 and 1, whereas the Boolean logic truth table of the XOR operator corresponds to multiplication for -1 and 1 when mapped to 0 and 1 (with an irrelevant sign inversion on the output)[2].

1.3.2 Unipolar Signal and Bipolar DLLO

With a unipolar signal, using a bipolar DLLO improves the electrical power signal-to-noise ratio (SNR) of the bitstream PC-CAML by about 2.5 dB for low signal counts compared to that of the unipolar DLLO as shown by the theoretical and Monte Carlo simulation results presented in this paper. Theoretically, there should be a 3 dB improvement for the bipolar DLLO from the elimination of the signal power loss to the DC component of the intermediate frequency (IF) spectrum that occurs with the unipolar DLLO. However, at low signal counts this improvement is partially offset by a higher quantization noise level for the bipolar DLLO compared to that of the unipolar DLLO as explained in section 2.3. At moderate signal counts before saturation effects occur, the simulation results indicate an SNR improvement of about 3 dB using a bipolar DLLO because the signal shot noise dominates over the quantization noise. At high signal counts after the onset of saturation, the SNR improvement using the bipolar DLLO diminishes.

Figure 3 shows the concept diagram for the implementation of the bitstream PC-CAML with a bipolar DLLO and a unipolar signal. For the bipolar DLLO, the chirped square wave LO consists of a single sign bit representing the polarity of the LO. The output of the photon counting detector receiving a chirped AM signal is a constant amplitude unipolar count. This signal count pulse is input to an edge-triggered pulse detector which outputs a very short single value bit unipolar digital logic level pulse. The digital mixing of the bipolar DLLO and the unipolar signal

---

2 The truth table for the Exclusive NOR (XNOR) gate corresponds exactly to multiplication for -1 and 1 when mapped to 0 and 1, but Bjorndal, et. al. [ref 15-18], use an XOR gate which induces a sign inversion in all the results. The sign inversion corresponds to a 180 degree phase shift, which is irrelevant, and the XOR has one less logic element (the NOT logic element), so the XOR gate is preferred.

logic level count pulses is implemented by assigning in each sample time the DLLO's sign bit to the sign bit of a 2-bit signed binary data register for which one bit represents a sign and the other bit represents a binary value, and assigning the signal's value bit to the binary value bit of this 2-bit signed binary data register, as shown in figure 3. The wideband, high speed 2-bit signed binary digital data from this 2-bit register can be either directly sent to storage and fully digitally processed, or sent through an analog or digital low/band pass filter in the IF band, the output of which is either digitized by a low sample rate analog-to-digital converter (ADC), or digitally down sampled to a low sample rate, respectively, as shown in figure 3. The low sample rate data is then sent to storage and digitally processed by the usual methods for chirped AM lidar.

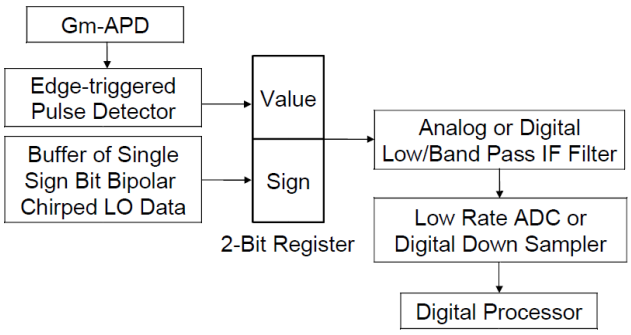

Figure 3. Bipolar DLLO and unipolar signal for Bitstream PC-CAML Concept Diagram

Note that although the description of the bipolar DLLO and unipolar signal count digital mixing is given above in terms of a sign bit and a value bit for simplicity and clarity, the 2-bit signed binary data can also use other representations of signed binary numbers, such as one's or two's complement representations, with the digital processing appropriate to those representations.

1.3.3 Unipolar Signal and Bipolar DLLO with Digital I/Q Demodulation

The single channel of digital mixing between the signal and DLLO described in the previous sections results in an electrical power SNR that is 3 dB lower than is achievable using digital in-phase and quadrature-phase (I/Q) demodulation since for the single mixer configuration "the thermal noise from the image sideband will always be present, so the noise floor will be 3 dB higher than could be achieved using I/Q mixers." [ref 21] This section describes a configuration with digital I/Q demodulation with the bipolar DLLO to improve the signal-to-noise ratio (SNR) by 3 dB compared to that for the single digital mixing channel with the bipolar DLLO.

Figure 4 shows a block diagram for the bitstream PC-CAML configuration with a unipolar signal and a bipolar DLLO with digital I/Q demodulation. In figure 4, the constant amplitude, single-bit binary output count of the Gm-APD detector is input to an edge-triggered pulse detector which outputs a shorter binary digital logic level pulse to the value bit of two 2-bit registers for each of which one bit is the value bit and for each of which the other bit is the sign bit.

The sign bit of the first 2-bit register, which is the in-phase (I) channel register, is connected to the binary sign data stream of a bipolar chirped cosine DLLO signal, which can be generated and stored in a data buffer prior to operation of the lidar. The sign bit of the second 2-bit register, which is the quadrature-phase (Q) channel register, is connected to the binary sign data stream of

a bipolar chirped sine DLLO signal, which can be generated and stored in a data buffer prior to operation of the lidar. The DLLO data buffers may be circular buffers to enable continuous repetition of the DLLO waveform.

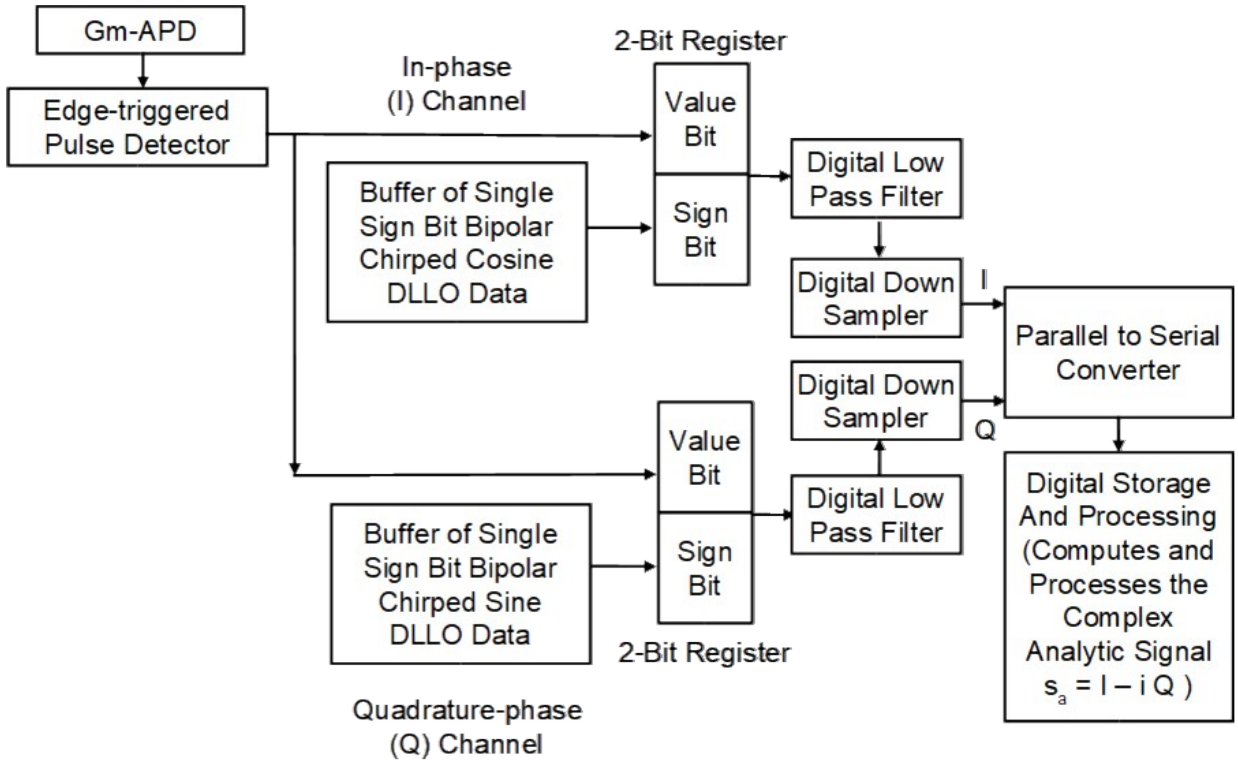

Figure 4. Bitstream PC-CAML receiver architecture with a unipolar signal and a bipolar DLLO with digital I/Q demodulation block diagram.

The signed digital data output from each 2-bit register are then sent to a corresponding digital low pass filter, the output of which is sent to a corresponding digital down sampler. The in-phase (I) and the quadrature-phase (Q) signals from the digital down samplers are input to a parallel to serial converter which outputs the I and Q signals digital data on a single serial line to the inputs of the digital data storage and processing subsystem. The digital signal processor (DSP) in this subsystem combines the real-valued I and Q data into the complex analytic signal data, $s_a = I–iQ$, where $i=(-1)^{½}$, and computes the power spectrum of s_a given by $S_a = |\text{cfft}(s_a)|^2$, where cfft(argument) is the complex fast Fourier transform (FFT) of the argument, and |expression| is the magnitude of the enclosed expression. The DSP finds peaks in the power spectrum S_a, which represent target returns. The frequency of a peak in S_a is proportional to a target range just as in the standard data processing for the standard PC-CAML.

Note that although the description of the bipolar DLLO and unipolar signal count digital mixing is given above in terms of a sign bit and a value bit for simplicity and clarity, the 2-bit signed data can also use other representations of signed binary numbers, such as one's or two's complement representations, with the digital processing appropriate to those representations.

1.3.4 Bipolar DLLO and Bipolar Received Signal using a Dual Unipolar Transmitted Signal

This section introduces a new bitstream PC-CAML transceiver architecture that combines two unipolar chirped signals, referred to as the dual unipolar (DU) signal, to form a single bipolar signal in the receiver. This bipolar signal is mixed with the bipolar DLLOs in the in-phase (I) digital mixing and quadrature-phase (Q) digital mixing channels for digital I/Q demodulation for improved signal-to-noise ratio (SNR) compared to that when using a single unipolar signal.

The simulation results presented in section 4 of this paper indicate an SNR improvement for the DU chirped sinusoidal signal bitstream PC-CAML compared to that of the unipolar chirped sinusoidal signal bitstream PC-CAML (both with bipolar DLLOs and digital I/Q demodulation) of from about 3.5 dB to about 7 dB for signals below the onset of receiver saturation, depending on the speckle diversity M and the signal level, and an improvement for maximum achievable SNR of about 13.5-16 dB, depending on M, if the receiver is allowed to saturate.

It is well known that since there cannot be negative optical power or intensity, the chirped AM (aka intensity modulation (IM)) optical signal is naturally unipolar. It is also well known that the unipolar chirped AM signal has an electrical power SNR that is a factor of 4 (6 dB) lower than that of an equivalent bipolar signal due to a 3 dB loss of signal power to the DC component and a 3 dB lower peak power as discussed in references 2-4.

In order to recover the SNR losses due to the unipolar nature of the chirped AM optical signal, the new dual unipolar (DU) signal technique was invented by the author and is presented herein. In this new technique, there are two optical signal channels, either split from one source prior to modulation, or from two different modulated sources. The modulation for channel 1 consists of the positive amplitude portions of a bipolar chirped sinusoid or square wave, between which there are zeros (no signal) where the negative amplitude portion of the bipolar chirped waveform was. The modulation for channel 2 consists of the negative amplitude portions of the same bipolar chirped sinusoid or square wave, between which there are zeros (no signal) where the positive amplitude portion of the bipolar chirped waveform was, but inverted in polarity to be a positive unipolar signal.

Each optical signal channel must be tagged uniquely so that they can be separated cleanly from each other in the receiver after having been combined into a single transmitted beam. This tagging can be done by each channel having a different optical carrier frequency/wavelength from each other or having orthogonal polarizations with respect to each other, for example.

Using orthogonal polarizations for tagging the channels is problematic since the target and/or the propagation medium may be depolarizing. Thus, only wavelength tagging is discussed.

For wavelength tagging, the optical carriers at two different wavelengths can be generated from two different sources, or from a single source followed by a frequency/wavelength shifter such as an acousto-optic modulator (AOM), electro-optic modulator (EOM), frequency doubler, Raman amplifier, or parametric amplifier, for example. The requirement on the wavelength difference between the two channels is that it is large enough that the two channels' optical spectra do not overlap. It is not necessary that the two wavelengths be in the same optical waveband since

different detector types with different spectral responses may be employed in the receiver. However, it may be simpler to use the same type of detector for each channel, in which case, the two wavelengths should be in the same spectral response waveband as the detector.

The use of a low cost, directly current modulated, low power, continuous wave (cw) semiconductor laser as the optical source for each wavelength channel is an attractive option. The optical linewidth of each laser needs to be narrow enough to minimize losses in the receiver's narrow band optical filters, but a temporally coherent single-frequency laser is not required. The wavelength separation between the two sources also needs to fit within the gain bandwidth of the optional optical amplifier used to increase the transmitted optical power, if needed, after the two channels are combined into a single beam for transmission.

On the order of one to a few nanometer filter linewidths are typically used with photon counting detectors in the presence of daytime solar backgrounds. The laser linewidths would need to be about half of the filter linewidth or less to insure good transmission through such filters in the presence of manufacturing tolerances on both the laser and the filter center wavelengths and linewidths, and to provide margin for optical Doppler frequency shifts for fast moving targets.

The difference between the two wavelengths should be at least a few times the filter linewidth to minimize spectral overlap so the two wavelengths can be cleanly separated in the receiver.

A representative set of parameters might be on the order of 0.5 nm laser linewidth, 1 nm filter linewidth, and 8 nm wavelength separation between the center wavelengths. The total bandwidth of less than 10 nm for the two sources in this case is well within the typical gain bandwidths of tens of nanometers for semiconductor and fiber optical amplifiers. A dichroic beamsplitter with no more than 7 nm edge steepness to combine/separate the two wavelengths is within the current capabilities of commercially available multilayer interference filters. Even smaller wavelength separations could be used with gratings or holographic filters for bulk optics, or other wavelength division multiplexing (WDM) de-multiplexing (demux) technologies in waveguides.

Figure 5 shows block diagrams for the transceiver architecture for the bitstream PC-CAML with a dual unipolar signal and bipolar DLLOs with digital I/Q demodulation using wavelength tagging. Figure 5 (a.) shows the transmitter architecture block diagram, and 5 (b.) shows the receiver architecture block diagram. The modulation waveforms are also illustrated in figure 5.

In figure 5 (a.) a digital chirped signal generator outputs the same, synchronized digital bipolar chirped sinusoidal or square wave signal on two channels. Digital signal processing circuitry in channel 1/2 retains the positive/negative amplitude portion of the bipolar chirped signal and replaces the negative/positive amplitude portion with zeros, respectively. Digital signal processing circuitry in channel 2 then inverts the polarity of the waveform.

A digital-to-analog (D/A) converter and analog driver circuitry in each channel converts the resulting unipolar waveform for each channel into a drive current that modulates the output power of the low power continuous wave (cw) semiconductor laser source in that channel. The laser in channel 1 operates at wavelength 1 ($\lambda 1$), and the laser in channel 2 operates at wavelength 2 ($\lambda 2$). An optical beam combiner combines the laser outputs at the two wavelengths

into a single beam. Note that the difference in path delays between the two channels needs to be less than a small fraction of the smallest period in the chirp waveform to maintain synchrony between the waveforms in the two channels.

The single two-wavelength beam with the combined channels 1 and 2 waveforms is amplified by an optical amplifier and transmitted through transmitter beam shaping optics to the targets.

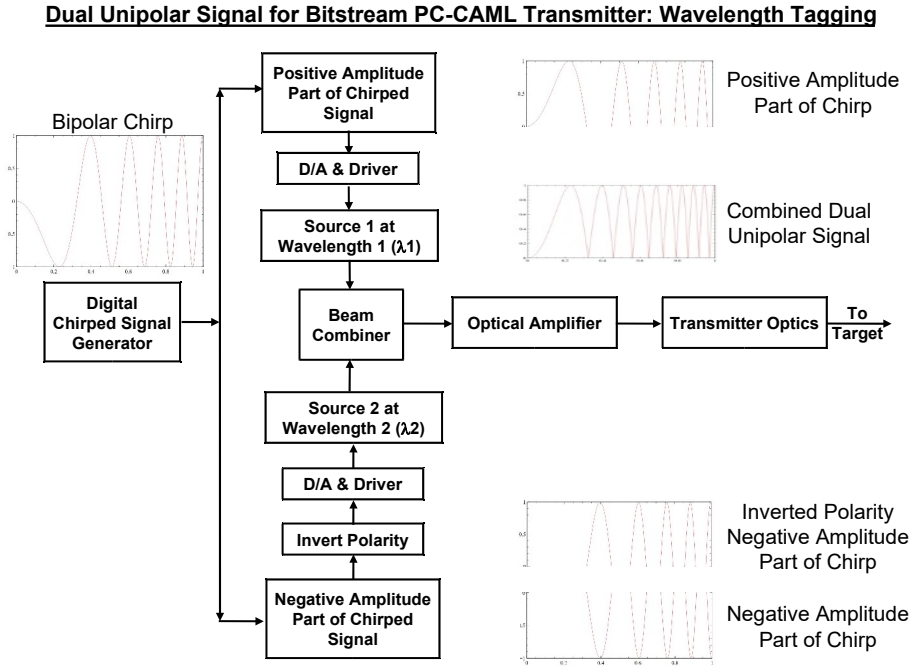

(a.)

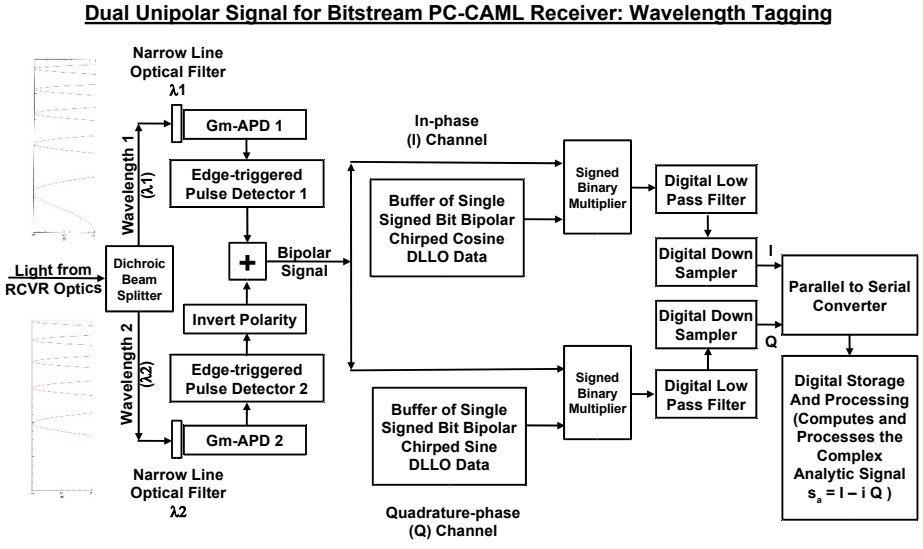

(b.)

Figure 5. Bitstream PC-CAML with a Dual Unipolar Signal using wavelength tagging transceiver architecture block diagram (a.) transmitter architecture block diagram and (b.) receiver architecture block diagram.

In figure 5 (b.), the light from the receiver optical system is split by a wavelength splitting device, such as a dichroic beam splitter, into two separate wavelength channels, one centered at wavelength 1 of transmitter channel 1 and the other centered at wavelength 2 of transmitter channel 2. The received light in each channel is transmitted through a narrow line optical filter centered at the center wavelength of that channel. Note that the optics in the transmitter and receiver systems may be fiber optical, waveguide and/or bulk optical components.

The filtered received light in each channel is detected by a Gm-APD photon counting detector. In each channel, the constant amplitude output count of the Gm-APD is input to an edge-triggered pulse detector which outputs a shorter single bit binary digital logic level pulse. The output of the edge-triggered pulse detector in channel 2 is inverted in polarity, and then added to the output of the edge-triggered pulse detector of channel 1, resulting in the bipolar received signal plus noise signed binary digital data.

The edge-triggered pulse detector allows the single-bit signal pulses to be much shorter than the count pulses output by the Gm-APD, which may be longer than desired due to the dead-time. The edge-triggered pulse detector's output pulse can be as short as a single clock pulse.

The bipolar signal plus noise signed binary digital data is duplicated so that one copy is routed to the in-phase (I) channel and the other copy is routed to the quadrature-phase (Q) channel. The bipolar signal plus noise signed binary digital data in each I/Q channel is multiplied by the bipolar digital logic local oscillator (DLLO) signed binary digital data of the corresponding channel. This signed binary multiplication may be implemented using a bipolar Boolean exclusive OR (XOR) or exclusive NOR (XNOR) binary digital logic gate, or using any other signed binary digital processing method. The bipolar DLLO data in each channel can be generated and stored in a data buffer prior to operation of the lidar. The DLLO data buffers may be circular buffers to enable continuous repetition of the waveform.

The signed binary digital data output from each multiplier are then sent to a corresponding digital low pass filter, the output of which is sent to a corresponding digital down sampler. The low pass filtering is required prior to the down sampling to prevent aliasing of higher frequency components and noise.

The in-phase (I) and the quadrature-phase (Q) signals from the digital down samplers are input to a parallel to serial converter which outputs the I and Q signals digital data on a single serial line to the inputs of the digital data storage and processing subsystem. The digital signal processor (DSP) in this subsystem combines the real-valued I and Q data into the complex analytic signal data, $s_a = I - iQ$, where $i=(-1)^{½}$, and computes the power spectrum of s_a given by $S_a = |\text{cfft}(s_a)|^2$, where cfft(argument) is the complex fast Fourier transform (FFT) of the argument, and |expression| is the magnitude of the enclosed expression. The DSP finds peaks in the power spectrum S_a, which represent target returns. The frequency of a peak in S_a is proportional to a target range just as in the standard data processing for the standard PC-CAML.

The bitstream PC-CAML with a dual unipolar signal and bipolar DLLOs with digital I/Q demodulation architecture discussed in this section adds complexity to the transmitter and receiver compared to the architectures presented in the previous sections. Whether or not this

additional complexity is worth the improved SNR will have to be decided as part of system trade studies for particular systems and their applications.

1.4 Inherent Digital Received Signal for PC-CAML

For the normal unipolar AM signal, the constant amplitude output of the Gm-APD regardless of the intensity of the received optical signal makes its output inherently single-bit binary, i.e., there is either a count, or there is no count. For the dual unipolar AM signal, the output in each Gm-APD receiver channel is also single-bit binary, but the channel corresponding to the negative portion of the bipolar signal is inverted to be negative so that the signal from combining the two channels is a bipolar signed binary digit, i.e., either -1 or 1. Thus, the bitstream PC-CAML may operate with either a chirped sinusoidal or chirped square wave transmitted waveform without requiring any additional thresholding and/or limiting in the receiver to convert a sinusoid to a square wave, as needed in the bitstream radar for a transmitted chirped sinusoidal signal.

1.5 DLLO Waveforms

The DLLO for the bitstream PC-CAML may be either a single-bit (signed for the bipolar case) chirped square wave or a single-bit (signed for the bipolar case) sampled chirped sinusoid. The advantage of having a single-bit sampled chirped sinusoidal DLLO instead of a single-bit chirped square wave DLLO is that whether the signal is a chirped square wave or a chirped sinusoid, mixing the signal and the DLLO will not produce harmonics in the IF spectrum. For a single-bit sampled chirped sinusoidal DLLO, the single-bit sample pulses may be, for example, pulse width modulated (PWM) or pulse density modulated (PDM) by the amplitude of the analog chirped sinusoid. The single-bit sampling of the chirped sinusoidal DLLO waveform may be uniform or non-uniform.

In the case of uniform sampling, the single-bit sampling rate must be many times the sampling rate of an equivalent multi-bit digitizer to retain the same signal-to-quantization-noise ratio (SQNR). [ref 22]. For example, according to equations 2.6, 3.8, and 3.9, and figure 3.9 in reference 22, to attain an SQNR of about 50 dB (8-bit equivalent SQNR), the sampling rate for single-bit sampling with third-order noise shaping must be about 11 times greater than the 8-bit sampling rate.[ref 22, pp. 10, 31-32] Thus, for a 1 GHz maximum chirp frequency, the 8-bit Nyquist sampling rate would be 2 GHz, and the required single-bit sampling rate with third-order noise shaping would be at least 22 GHz to achieve the same SQNR. Such a high sampling rate is not practical for inexpensive silicon CMOS ROICs. Therefore, uniform single-bit sampling of the chirped sinusoidal LO does not seem to be worthwhile to investigate further at this time.

In the case of non-uniform sampling, the average single-bit sampling rate may be much lower than the Nyquist sampling rate if an alias-free sampling scheme, such as a random Poisson point process sampling scheme [ref 23] or an additive random sampling (ARS) scheme [ref 24], is used, and if the clock rate is at least twice the highest chirp frequency. [ref 25] However, random sampling introduces noise into the LO as discussed in detail by Luo. [ref 25]. In addition, when the number of 1's in the random sampling of the LO exceeds half of the total number of available samples, the apparent modulation depth of the chirped sinusoidal LO diminishes, going to zero when all of the samples are filled with 1's, for the same reason that this happens to the chirped

sinusoidal signal that is single-bit sampled by the Gm-APD when the Gm-APD approaches saturation as explained in section 2.1 below. Initial Monte Carlo simulations verified the significant reduction of the IF signal's SNR due to the additional LO noise and apparent modulation depth loss. Therefore, random single-bit sampling of the chirped sinusoidal LO does not appear to be worthwhile to investigate further at this time.

Therefore, this paper discusses just a chirped square wave DLLO.

1.6 Harmonics and their Mixing Products

At signal levels well below receiver saturation with a chirped sinusoidal signal, the bitstream PC-CAML will be mixing a randomly sampled chirped sinusoidal modulation of the received signal count rate with a chirped square wave LO. Just as for the linear response receiver based CAML with a chirped sinusoidal signal and chirped square wave LO, this does not produce harmonics in the mixed signal's intermediate frequency (IF) power spectrum. However, when the transmitted waveform is a chirped square wave or when the receiver starts to saturate so that it "squares off" the received waveform, the bitstream lidar will be mixing a chirped square wave signal and a chirped square wave LO which will produce odd-order harmonics and their mixing products.

These odd-order harmonics and their mixing products also occur in the bitstream radar, for which both the signal and LO are chirped square waves. Bjorndal, et. al., have shown three ways of dealing with these odd-order harmonics to mitigate their effects in bitstream radar by suppressing them or even by utilizing them for improved range resolution [ref 15-18], and which can also be used in the bitstream PC-CAML:

1. Known pseudorandom or random dithering of the chirp signal's phase with or without noise shaping to spread out the harmonics over the spectrum
2. Transmitted waveform additional delay to shift the harmonics beyond the intermediate frequency (IF) corresponding to the desired unambiguous range
3. Detection at a harmonic frequency for improved range resolution.

As Bjorndal points out, dithering the chirp signal's phase can spread out the energy of the harmonics over the power spectrum, but this increases the noise floor. [ref 18, pp. 12, 56, 62-65]

1.7 Aliasing

Dithering can also be used to address the issue of aliasing. As Bjorndal states "If we sample, either by transmitting a sampled bitstream, or sample on the receiver without an anti-aliasing filter then anything above the sample rate is going to fold down...Avoiding aliasing on the receiver side is best done with an analog low-pass filter and a multi-bit ADC ..., while aliasing on the transmitter can be mitigated with intentional dithering..." [ref 18, p.56] Use of an anti-aliasing filter with a multi-bit ADC in the wideband signal path on the receiver, however, complicates the receiver, and dithering on the transmitter complicates the transmitter.

Fortunately, at signal levels well below saturation, the quantum randomness of the photon stream and noise counts in the PC-CAML provides nonuniform random sampling of the transmitted waveform, which can eliminate the aliasing inherent in uniform sampling. The Nyquist sampling

theorem applies only to uniform sampling. For example, Beutler showed that any spectral distribution is alias-free if randomly sampled by a Poisson point process. [ref 23]

However, for the bitstream PC-CAML, as the signal level increases into receiver saturation so that all the available samples start filling up with ones, the sampling becomes more like uniform sampling and aliasing can occur.

Gatt, et. al., show that the lidar signal counts from a photon counting Gm-APD have a negative binomial distribution rather than a Poisson distribution due to the speckle diversity. [ref 26, pp. 3264-3266] (Note that the form of the negative binomial distribution used in Gatt, et. al., is also called the Gamma Poisson (mixture) distribution. [ref 27-28]). They also model the noise counts with a Poisson distribution. The resulting signal plus noise counts for the Gm-APD based lidar have a Negative Binomial Plus Poisson (NBPP) distribution resulting from the convolution of the negative binomial and Poisson distribution given in Gatt, et. al.. [ref 26, p. 3265] When the number of signal photoelectrons per matched filter impulse response time are much less than the speckle diversity, M, the counts distribution is approximately Poisson [ref 26, p. 3265], so the alias-free property of Poisson sampling holds in this limit.

The author is not aware of any prior work showing that an NBPP point process has the alias-free property in general. Determining whether or not the NBPP point process provides alias-free random sampling in general is beyond the scope of this paper and is suggested for future work. However, the counts from the Gm-APD can be viewed as the result of an additive random sampling (ARS) process. An ARS process is defined by having sample times given by $t_n = t_{n-1} + \tau_n$, where n is an integer, and $\{\tau_n\}$ is a family of independent identically distributed positive random variables. This says that the current count sample time is the previous count sample time plus a random delay time, which is the case for the Gm-APD counts for PC-CAML. An important result for our purposes from the thesis of King Chuen Lo is that an ARS process is alias-free for any distribution of $\{\tau_n\}$ for a sampling duration T larger than T_a , where T_a depends on the probability density function of τ. [ref 24, p. 52]

Luo points out in his thesis that the foregoing tacitly assumes that the time intervals $\{\tau_n\}$ are continuously distributed. [ref 25, p. 99] However, in a real sampled system, the sample time intervals are discrete at the clock time interval, Δ. Luo shows that for discrete clock time intervals of Δ, additive random sampling is alias-free only if the signal is band-limited in $[-1/2\Delta , 1/2\Delta]$. [ref 25, p. 100] Luo also shows that for exponentially distributed $\{\tau_n\}$, which is the case for a Poisson point process, for such a band-limited signal, the sampling is alias-free for any number of counts accumulated. [ref 25, pp. 80 and 84-86]

Thus, the average count rate for an ARS process can be much lower than the Nyquist sampling rate for the signal bandwidth if a sufficient number of additive random counts are accumulated, but the clock rate must be at least twice the signal bandwidth for alias-free sampling.

1.8 Dead-Time and Count Pulse Rise Time Limitations on Signal Bandwidth

One might think that the chirp's maximum frequency would be limited to no more than $1/2t_d$, where t_d = the dead-time. As Redman, et. al., demonstrated, however, it is the rise-time of the

count pulse (assuming a sufficient sampling frequency and clock accuracy), not the dead-time, that sets the upper frequency limit for PC-CAML with pre- or post-detection mixing. [ref 2-4].

On the other hand, for OEM mixing by modulating the bias voltage of the Gm-APD directly with a square-wave LO signal, the highest useful chirp frequency is limited by the Gm-APD dead-time. [ref 2-4, 8-9, 13] If, however, the LO is applied by modulating the gate open duration of the Gm-APD such that the gate open duration is proportional to the amplitude of a sinusoidal LO, then the dead-time limit on the highest chirp frequency can be eliminated by setting the longest gate open duration, Δt_g, and the shortest time sample interval between starts of opening the gate, t_{gs}, such that $t_{gs} - \Delta t_g > t_d$, where t_d is the dead-time. [ref 11, p. 11802] In this case, the highest chirp frequency is limited by the smallest gate duration that can be applied to the Gm-APD.

Luo's analysis discussed above does not take into account the finite rise-time of the edges of the count pulses. If the clock time interval, Δ, is much larger than the count pulse rise-time, then the signal must be band-limited within $[-1/2\Delta , 1/2\Delta]$ as stated by Luo. If, however, Δ is less than or equal to one-half the count pulse rise-time, then the signal bandwidth must be less than or equal to half the bandwidth of the count pulse's rising edge. When the count pulse rise-time equals 2Δ, so that the count pulse rising edge is sampled at the Nyquist rate, then the signal must be band-limited within $[-1/2t_r,1/2t_r] = [-1/4\Delta , 1/4\Delta]$, where t_r is the count pulse rise-time.

Gatt, et. al., state "...a signal with intrinsic diversity M behaves much like a Poissonian signal when $m_s \ll M$. That is to say, quantum noise dominates over speckle noise" where m_s is the average number of signal photoelectrons per matched filter impulse response time and M is the speckle diversity. [ref 26, p. 3265] Usually, for well designed photon counting lidars, in order to prevent receiver saturation, transmitter power and/or receiver throughput control will be used to enforce $m_s << M$. Also for well designed photon counting lidars, measures such as using narrow band optical filters and low dark count rate Gm-APDs, will be taken to insure that $m_n << m_s$, where m_n is the average number of noise photoelectrons per matched filter impulse response time, otherwise, the arm probability (PA) and signal-to-noise ratio (SNR) will be too low for practical operation. In addition, the average total number of photoelectrons in a dead-time, t_d, given by $m_d = (m_s+m_n)\cdot(t_d/t_{imf})$, where t_{imf} is the matched filter impulse response time, should be kept to no more than the order of about unity in order to maintain a high PA and SNR. (See reference 26 for more detailed discussions of m_s, m_n, m_d, arm probability and SNR.)

Therefore, usually for a well designed bitstream PC-CAML with transmitter power and/or receiver throughput control, and low noise count rate, the signal plus noise will be well approximated by Poisson distributed signal plus noise, and the signal spectrum will be alias-free for any accumulation duration if the signal's bandwidth is within the limits set by the clock time interval and the count pulses' rise-time as discussed above. In addition, since the counts form an ARS process, even for high count rates, but count rates still below receiver saturation, the spectrum will be alias-free for a sufficient number of accumulated counts if the signal bandwidth, count pulse rise-time, and sampling clock time interval meet the requirements discussed above.

1.9 Detection at a Harmonic Frequency for Improved Range Resolution

When using a chirped square wave signal, detection at a harmonic frequency for improved range

resolution can be done for processing bitstream PC-CAML data in the same manner as described by Bjorndal, et. al., for bitstream radar [ref 16-18], but further investigation into that technique is beyond the scope of this paper and is suggested for future work. If the harmonics are to be used for improved range resolution, the additional bandwidth of the harmonics to be used for this purpose must be included in the signal bandwidth limits for alias-free sampling discussed above.

1.10 Transmitted Waveform Delay for Shifting Harmonics Beyond the Unambiguous Range

Since dithering increases the noise floor and is not needed for anti-aliasing for a well designed bitstream PC-CAML operating well below receiver saturation, and since detection at a harmonic frequency is beyond the scope of this paper, in this paper, just the ability of a transmitted waveform delay to shift the frequencies of the harmonics beyond the desired unambiguous range frequency for the bitstream PC-CAML with a DLLO is demonstrated with simulation results.

The additional delay on the transmitted waveform is equivalent to an advance of the LO waveform. Therefore, the additional transmitted waveform delay can be implemented by starting the LO waveform earlier than the start of the transmitted waveform and extending the LO's chirp duration and frequency along the chirp's temporal slope for complete overlap with the round-trip delayed received chirp signal's duration.

2. Bitstream PC-CAML with a DLLO SNR Theory

The purpose of this paper is to introduce the new bitstream PC-CAML with a DLLO concept and to show through simulation results how it works. The purpose of this paper is not to develop a comprehensive theory of operation for the new concept, so the initial SNR theory presented herein is approximate and has a limited range of applicability to the new concept. Thus, an improved theory needs to be developed in future work.

The initial electrical power signal-to-noise ratio (SNR) theory used herein for the bitstream PC-CAML with a DLLO concept is derived from the SNR theory for photon counting Gm-APDs developed by Gatt, Johnson, and Nichols. [ref 26, pp. 3265-3270] The theory developed by Gatt, et. al., is for detection of pulsed lidar returns. This theory, however, can be applied to the bitstream PC-CAML as simulated in Mathcad®[3] by making the following adjustments:

1. Reducing the SNR by the product of three SNR reduction factors to account for losses due to the use of unipolar waveforms and due to not using I/Q demodulation in the bitstream PC-CAML as discussed in the papers presenting the original PC-CAML concept by Redman, Ruff, and Giza [ref 2-4].:
    a. a signal SNR reduction factor of 4 for a unipolar signal (consisting of a factor of 2 loss to the DC component and a factor of 2 reduction in peak signal power for a unipolar signal) or 1 for a dual unipolar/bipolar signal
    b. an LO SNR reduction factor of 2 for a unipolar LO or 1 for a bipolar LO
    c. an I/Q SNR reduction factor of 2 if I/Q demodulation is not used or 1 if I/Q demodulation is used.

---

3 Mathcad® is a registered trademark of PTC Inc. or its subsidiaries in the U.S. and in other countries.

2. Adding quantization noise due to the single-bit quantization
3. Setting the arm probability, PA, in the SNR equations of Gatt, et. al., [ref 26, pp. 3268-3270] to the steady state arm probability PA_{ss} in Gatt, et. al., [ref 26, p. 3266, equation (15)] since the duration of the chirp signal and therefore, the integration time of the resulting IF signal effected by the computation of the power spectrum of the IF signal, are typically very much longer than both the matched filter impulse response time and the Gm-APD dead-time in practical PC-CAML systems. However, the total number of photoelectrons within the dead-time, given my m_d, used in calculating the stead state arm probability is altered for reasons explained below.
4. Multiplying the theoretical SNR by the square of the modulation index, μ, of the chirped waveform account for the SNR loss due to a modulation index less than 1. Note that for the simulated chirped waveform used in the simulations, the modulation index is 1.
5. Multiplying the theoretical SNR by the Hann efficiency $\eta_{Hann} = 10^{-0.1761}$ to account for the Hann window processing loss. The Hann window is applied to the data in the simulations (see section 3) to reduce sidelobes. In general, there would be an additional loss when the peak of the IF signal is at a frequency that is between sample frequencies in the power spectrum. This is called the scalloping loss efficiency, which is given by $\eta_{Scallop} = 10^{-0.142}$ for the worst case scalloping loss. However, in the simulations, the peak of the IF signal is chosen to be at a sample frequency, in which case $\eta_{Scallop} = 1.0$.

Equation (41) from Gatt, et. al., [ref 26, p. 3269] modified as described above is equation (1.):

$$SNR_{theory} = \frac{\eta_{\text{Hann}}\,\eta_{\text{Scallop}}\,\mu^2 N_s PA_{SS}\left[1-\left(\frac{M}{M+m_s}\right)^M\right]^2}{F_S \cdot F_{LO} \cdot F_{IQ}\left[1-e^{-\left(m_n+m_{qn}\right)}\left(\frac{M}{M+m_s}\right)^M\right]\left[1-PA_{SS}\left[1-e^{-\left(m_n+m_{qn}\right)}.\left(\frac{M}{M+m_s}\right)^M\right]\right]} \qquad (1.)$$

where η_{Hann}= Hann efficiency = $10^{-0.1761}$.

η_{Sc} = Scalloping efficiency = $10^{-0.142}$ at worst and = 1 at best (it is 1 for the simulations).

μ = modulation index for the unipolar chirped AM signal, $I_S(t) = I_{DC}[1+ \mu\cos(\omega(t)t)] = [I_{max} - I_{min}] / [I_{max} + I_{min}]$, where I_{max} and I_{min} are the maximum and minimum intensities of the modulated chirped AM signal light, respectively, and $I_{DC} = [I_{max} + I_{min}]/2$ = the mean intensity of the modulated chirped AM signal light. (Note: $m_s \propto I_{DC}$ and $\mu = [m_{s\_max} - m_{s\_min}]/[2m_s]$).

N_s = Number of matched filter impulse response times accumulated over the chirp duration. The matched filter impulse response time for the chirp is given by 1/B where B is the chirp bandwidth given by |fstop – fstart|, fstart is the frequency of the AM at the start of the chirp and fstop is the frequency of the AM at the end of the chirp. When a Hann(ing) window is used to process the data, the matched filter impulse response time is increased to 1.44/B.

PA_{ss} = the steady state Arm Probability = $1/(1+m_d)$, where $m_d = m_{do}/\alpha$, where m_{do} = the original calculation of the mean total number of photoelectrons in a dead-time = $\psi_0 \cdot t_d$, where ψ_0 is the original mean steady state total photoelectron flux and t_d is the dead-time, and α is a factor to compensate for the steady state arm

probability underestimating the exact calculation of the arm probability for portions of the waveform, as explained below.

M = speckle diversity

F_S = SNR reduction factor due to signal polarity = (4 for the unipolar signal, 1 for the dual unipolar/bipolar signal)

F_{LO} = SNR reduction factor due to LO polarity = (2 for the unipolar LO, 1 for the bipolar LO)

F_{IQ} = SNR reduction factor depending on whether or not I/Q demodulation is used = (2 for not using I/Q processing, 1 for using I/Q processing)

m_s = average number of signal photoelectrons received by the Gm-APD per impulse response time prior to reduction by the arm probability

m_n = average number of noise photoelectrons per impulse response time prior to reduction by the arm probability (includes all of the additive noise sources except for quantization noise)

m_{qn} = the average number of quantization noise photoelectrons per impulse response time.

The effects on the theoretical SNR of the dead-time and Gm-APD receiver saturation are incorporated via the arm probability. Since for the bitstream PC-CAML, the duration of the chirp signal and the matched filter duration for the chirp signal, which is the inverse of the chirp bandwidth, are typically very much longer than the Gm-APD dead-time in practical PC-CAML systems, the steady state arm probability, PA_{ss} , equation (15) from Gatt, et. al. [ref 26 p. 3266], is the starting point for determining the arm probability in the SNR theory for the bitstream PC-CAML. However, calculations of the exact arm probability using the equations from Gatt, et. al. [ref 26 pp. 3266-3267, equations (12), (18) and (25)] indicate that the exact arm probability averaged over segments of the signal substantially exceed the steady-state arm probability given in Gatt, et. al. [ref 26 p. 3266, equation (15)]. Unfortunately, due to computer memory limitations and computation time, the calculation of the exact arm probability could be performed over only short segments of the signal, but not the entire signal. Therefore, the value of the mean total number of photoelectrons in a dead-time given by m_d in the steady-state arm probability equation is modified by dividing the original value of m_d, designated by m_{do}, by a factor $\alpha > 1$ such that $m_d = m_{do}/\alpha$, which has the effect of increasing the arm probability. Thus, the equation for the steady state arm probability becomes

$$PA_{ss} = 1/(1+m_d) = 1/(1+m_{do}/\alpha) = \alpha/(\alpha+m_{do}), \text{ where } \alpha > 1 \qquad (2.)$$

Since $m_{do} > 0$, this modified steady-state arm probability is always between 0 and 1, inclusive, for any value of α., as it should be. When $m_{do} >> \alpha$, $PA_{ss} \sim \alpha/m_{do}$, which is α times the original steady state arm probability for large m_{do}, which is approximately $1/m_{do}$ in the same limit.

Initially, this indicated that α should be set to PA_{exact}/PA_{ss}, where PA_{exact} is the result of the exact calculation of the arm probability over some segments of the signal waveform. However, this ratio varied with signal levels and durations. Using a large value of this ratio for α being constant with signal level caused the SNR to be overestimated for low signals, but using a low value for α caused the SNR to be underestimated for large signals. Therefore, α was chosen to be a function that increased from 1 at zero mean total counts per dead-time, so that PAss is equal to the

original steady state arm probability at that point, to e (2.718) at one mean total counts per dead-time (since the Gm-APD's maximum number of possible counts per dead-time is one) as follows:

$$\alpha(\text{counts\_tot\_td}) = e^{\text{counts\_tot\_td}}, \quad (3.)$$

where counts_tot_td = the original total (signal + noise) counts in the dead-time

$= m_{do} \cdot PA_{ss0}$, where $PA_{ss0} = 1/(1+m_{do})$

Since the measured counts are after the reduction of the number of photoelectrons by the arm probability, we must calculate the number of photoelectrons for input to the SNR theory from the measured counts using the following equations derived from the PA_{ss} equation:

$$m_{do} = \text{counts\_tot\_td}/(1-\text{counts\_tot\_td}), \quad (4.)$$

where counts_tot_td = the original total (signal + noise) counts in the dead-time

$= m_{do} \cdot PA_{ss0}$, where $PA_{ss0} = 1/(1+m_{do})$

$$m_d = m_{do}/\alpha(\text{counts\_tot\_td}) = \text{counts\_tot\_td}/(\alpha(\text{counts\_tot\_td})(1-\text{counts\_tot\_td})) \quad (5.)$$

$$= e^{-\text{counts\_tot\_td}}\text{counts\_tot\_td}/(1-\text{counts\_tot\_td})$$

In the experiment and simulations discussed below, the actual measured quantities are the total counts (signal plus noise) and the noise counts in the chirp duration, from which we deduce that the signal counts = total counts – noise counts and quantization noise counts = total counts/Fqn, where Fqn is a factor that depends on the type of modulation and demodulation (see section 2.3), and from these counts we deduce the corresponding number of photoelectrons based on the steady state arm probability. Therefore, from the original steady state arm probability equation, we have

$$m_{dn} = \text{counts\_noise\_td}/(1-\text{counts\_tot\_td}) \quad (6.)$$

where counts_noise_td = the original mean noise counts in the dead-time

$= m_{dn} \cdot PA_{ss0}$, where $PA_{ss0} = 1/(1+m_{do})$

$$m_{ds} = m_{do} - m_{dn} = (\text{counts\_tot\_td} - \text{counts\_noise\_td})/(1-\text{counts\_tot\_td}) \quad (7.)$$

$$m_{dqn} = m_{do}/F_{qn} \quad (8.)$$

Note that since the photoelectron arrivals are not correlated from sample to sample, the mean number of photoelectrons per sample duration can be used in equation (1) with N_s becoming the number of samples collected in the chirp duration rather than using the number of photoelectrons in a matched filter impulse response time. Since the sample duration and the dead-time were set equal for the simulations discussed below, in calculating the SNR from the theory given by equation (1.) for comparison to the simulation results, we can use the mean numbers of photoelectrons in a dead-time as given by equations (3-7). Therefore, the theoretical SNR curves and simulation SNR results discussed in section 4 are plotted together against the mean total number of counts within a dead-time. Note that the modified mean total number of photoelectrons within a dead-time, $m_d = m_{d0}/\alpha$, given by equation (4), is used only in calculating the steady state arm probability, PA_{ss}, as discussed above, and only the original mean number of photoelectrons calculated from the original counts and original unmodified steady state arm

probability, PA_{ss0}, as shown in equations (3) and (5-7), are used in all parts of the SNR theory equation (1) other than in the calculation of PA_{ss}.

This SNR theory does not include the effects of energy losses to higher order harmonics and their mixing products. This SNR theory includes the effect of the signal's modulation depth, but the simulations were run for a perfect 100% modulation depth for the chirped AM signals.

2.1 Sinusoidal Modulation Depth Loss Near Saturation for the Unipolar Sinusoidal Signal

As the mean number of total counts output by the Gm-APD per available sample with a duration of the dead-time, counts_tot_td, increases towards 1, the apparent modulation depth of the unipolar sinusoidal chirped AM waveform decreases due to the Gm-APD being able to output at most only a single count per dead-time causing the arm probability to decrease with increasing total number of photoelectrons in a dead-time. This nonlinear saturation of the receiver at high photoelectron arrival rates suppresses signal variance.[ref 26 pp. 3263, 3268 and 3271] For the unipolar sinusoidal signal, when the mean count rate is so high that on average a count is output for every sample, the single-bit count data stream approaches that of a constant, unmodulated signal corresponding to a modulation depth of zero and therefore, the SNR goes to zero.

For the fully modulated dual unipolar sinusoidal signal with wavelength tagging, in each channel, and for the fully modulated unipolar square wave signal, however, the samples where there are zero's in a channel's waveform are never filled by 1's for any signal level, and those samples can only have an occasional 1 due to noise at the low noise levels in the simulations and in a well designed PC-CAML. Thus, as counts_tot_td approaches 1, only the samples corresponding to the non-zero levels of the dual unipolar signal or the unipolar square wave signal in each channel become filled with 1's, causing the waveform in each channel to approach the uniformly sampled deterministic unipolar chirped square wave as counts_tot_td approaches 1. In the dual unipolar signal case, this then causes the combined received bipolar signal waveform to approach the uniformly sampled deterministic bipolar chirped square wave as counts_tot_td approaches 1. In the unipolar chirped square wave signal case, this then causes the received signal waveform to approach the uniformly sampled deterministic unipolar chirped square wave as counts_tot_td approaches 1. When this occurs, the floor of the power spectrum of the mixer output becomes dominated by sidelobes and perhaps aliasing, depending on the sampling rate and signal bandwidth, rather than dominated by noise for the low noise rates of a well designed PC-CAML.

These effects of Gm-APD receiver saturation on the chirped sinusoidal unipolar and dual unipolar, and unipolar chirped square wave waveforms are illustrated by the results from the Monte Carlo simulations shown in sections 3 and 4. These effects, however, are not included in the initial SNR theory represented by equation (1.), but should be included in future work on the theory.

2.2 Effects of Speckle Diversity depend on whether the Signal is Unipolar/Dual Unipolar and Sinusoidal/Square Wave

As shown by the Monte Carlo simulation SNR results in section 4, the value of the speckle

diversity, M, affects the SNR for the unipolar chirped sinusoidal signal as predicted by the SNR theory. However, the Monte Carlo simulation results also show that the value of M makes no significant difference in the SNR for a fully modulated unipolar chirped square wave signal, nor for a fully modulated dual unipolar chirped sinusoidal signal in contrast to the theory's predictions. The following is an untested conjecture to explain these results, but more work on the SNR theory is clearly needed.

For each channel of the fully modulated dual unipolar chirped sinusoidal signal, and for the fully modulated unipolar chirped square wave, where the signal is zero, there are no speckle induced signal fluctuations since there are no signal counts in those areas. Although the photon arrival rates will vary with the speckle amplitude fluctuations in the non-zero areas of the signal, since the mean intensity of the integrated speckle is independent of M, this may just look like additive random sampling of the those areas of the signal with a different distribution of random samples depending on M, which does not change the SNR. Therefore, for the fully modulated dual unipolar chirped sinusoidal signal and the fully modulated unipolar chirped square wave signal, the effect of the speckle induced signal amplitude fluctuations on the SNR is nearly eliminated.

For the fully modulated unipolar chirped sinusoidal signal, there is some signal everywhere except at the exact nulls of the waveform, so that the speckle induced amplitude fluctuations cause photon arrival rate fluctuations at almost all points on the signal, and these fluctuations are higher for lower M causing the SNR to be lower for lower M just as seen in the Monte Carlo simulation results and theory predictions for the unipolar chirped sinusoidal signal.

If this is true, then if the unipolar chirped square wave signal or the dual unipolar chirped sinusoidal signal were not fully modulated, there would be a small, but non-zero, signal level in the areas of the signal that would be zero otherwise. This small, non-zero signal level would be subject to speckle induced amplitude fluctuations, and the speckle induced amplitude fluctuations over the whole signal would then be detected as photon arrival rate fluctuations, which would reduce the SNR with increasing amplitude fluctuations corresponding to decreasing M. Extending the simulations for less than 100% modulation depth will provide a test of this conjecture and is suggested for future work.

2.3 Single-bit Quantization Noise

Lastly, noise due to single-bit quantization must be calculated to use in the SNR theory of equation (1.). The quantization noise is computed from the Signal-to-Quantization-Noise Ratio in dB ($SQNR_{dB}$) given by equation 2.38 of Bjorndal [ref 18, p. 40]:

$$SQNR_{dB} = 6.02*N_{bits} + 1.76, \text{ where } N_{bits} = \text{the number of bits of digitization.} \quad (9.)$$

which can be rewritten as

$$SQNR = 10^{(6.02*Nbits + 1.76)/10} \quad (10.)$$

The quantization noise per single bit is the reciprocal of the SQNR, and is given by

$$qn\_per\_bit = 10^{-(6.02*Nbits + 1.76)/10} \quad (11.)$$

The number of bits, N_{bits}, for input to equation (11.) for the intermediate frequency (IF) signal resulting from mixing the received signal and the DLLO is determined by the number of states, N_{states}, of the result of multiplying the signal and DLLO, and is given by the following:

$$2^{N_{bits}} = N_{states} \Longrightarrow N_{bits} \cdot \ln(2) = \ln(N_{states}) \Longrightarrow N_{bits} = \ln(N_{states})/\ln(2) \quad (12.)$$

When both the signal and DLLO are unipolar, the number of states of the mixed signal is 2, i.e., either 0 or 1, and from equation (12), $N_{bits} = 1$. Thus, from equation (11), for a single-bit unipolar signal and DLLO, the quantization noise per 1-bit count is then $10^{-0.778} = 1/6$. The average quantization noise photoelectrons per sample is the average number of signal plus noise photoelectrons per sample times qn_per_bit, and is given by the following equation in the simulations for the unipolar signal and DLLO case:

$$m_{qn\_avg} = m_{t\_avg}/6 \quad (13.)$$

where m_{qn_avg} = the average number of quantization noise photoelectrons per sample.

m_{t_avg} = the average number of total photoelectrons per sample.

When either or both the signal and DLLO are bipolar, the number of mixed signal states is 3, i.e., (-1,0,+1), where +/-1 occurs when the signal and DLLO count pulses are the same/opposite polarity, respectively, and 0 occurs when there is no signal count. In this case, $N_{bits} = \ln(3)/\ln(2) = 1.5849625$, $SQNR = 10^{1.1301474} = 13.4942$, and qn_per_bit = 1/13.4942.

The above calculation applies to the N_{bits} quantization noise for the mixed signal using the unipolar DLLO with the AND logic gate digital mixer. However, Klein states and shows that "… the logic function XOR results in the negative multiplication of two bipolar bit-streams, and the logic function AND results in the multiplication of two unipolar bit-streams...For the logic operation XOR, the standard deviation is doubled in comparison to the operations OR and AND...Due to the fact that the output bit stream changes from zero to one with XOR and only from 0.5 to zero or one with OR and AND, the scaling is expected to be a factor of two of the standard deviations from OR and AND to XOR." [ref 29]

Since for the electrical power SNR, the noise is given by the variance rather than the standard deviation, the quantization noise for the bipolar signal and/or bipolar DLLO is 4 times higher than that for the unipolar signal and unipolar DLLO with the same number of quantization bits. Therefore, for the bipolar signal and/or bipolar DLLO, the average number of quantization noise photoelectrons per sample is given by:

$$m_{qn\_avg} = 4 \cdot m_{t\_avg}/13.4942 = m_{t\_avg}/3.37355 \quad (14.)$$

where m_{qn_avg} = the mean number of quantization noise photoelectrons per sample in the simulations

m_{t_avg} = the mean number of total photoelectrons per sample in the simulations.

Thus, the average number of quantization noise photoelectrons per sample for a bipolar signal and/or bipolar DLLO is 1.78 times higher than when both the signal and DLLO are unipolar.

Note that the above calculations of the quantization noise are applicable whether or not I/Q

demodulation is employed since I/Q demodulation only effects the thermal noise, and the effect of I/Q demodulation on SNR is accounted for by the SNR reduction factor F_{IQ} in equation (1).

However, for the dual unipolar signal with bipolar LOs, and I/Q demodulation configuration, multiple channels contribute to the single-bit quantization noise in contrast to the unipolar signal configurations. For the dual wavelength, dual unipolar configuration, there are 2 channels because of the 2 GmAPDs, one for each wavelength.

Note that since the quantization noise for each channel is inherent in the digitization of the signals + noise in each channel in the simulations, the multiple channels' contributions to the quantization noise is naturally included in the simulation results. However, for the SNR theory, the multiple channels contributions to the quantization noise must be explicitly accounted for and computed.

The need to account for the quantization noise in each channel and the fact that the noise variances from each channel add to give the noise variance for the resultant signal from combining the channels, since the channels are uncorrelated, is discussed in reference 30.

For the bitstream PC-CAML, the transmitted chirped sinusoidal signal may be generated by analog electronics which would not introduce quantization noise. Alternatively, the chirped sinusoidal signal may be generated digitally and converted to an analog intensity modulation using a D/A converter. Quantization noise is generated on the transmitted signal in this latter case. However, typically a large bit depth (e.g., 8-bit to 32-bit) will be used in the digital signal generator so that the quantization noise in the generated signal will be negligible compared to that produced by the single-bit receiver.

In the receiver, the single-bit quantization produced by the Gm-APD introduces quantization noise.

The I and Q channels do not contribute to the quantization noise because the signed bits represent the chirped square wave LO exactly.

Therefore, there are a total of 2 channels of signed single-bit quantization for the wavelength tagging dual unipolar signal, one each from the two GmAPDs. For the unipolar signal cases, there is only one channel of single-bit quantization noise, from the one GmAPD.

Thus, for the unipolar signal cases, the number of single-bit quantization noise PEs are given fully by the equations presented above.

For the dual unipolar signal configuration, however, the quantization noise, which is a variance, given by the equations above must be multiplied by the number of channels contributing to the quantization noise, namely 2 channels for the dual unipolar wavelength tagging configuration.

Thus, $m_{qn\_avg} = 2{\cdot}4{\cdot}m_{t\_avg}/13.4942 = m_{t\_avg}/1.686775$ for the wavelength tagging dual unipolar signal configuration.

In the initial SNR theory, equation (1.), m_{qn} is set equal to the value of m_{qn_avg} for the simulations for which the SNR theory and simulation results are being compared.

3. Descriptions of the Simulations for Various Configurations

The equations and procedures used in the Monte Carlo simulations are discussed in the subsections of this section for the various configurations of unipolar signal with a unipolar LO or with a bipolar LO without and with In-phase and Quadrature-phase (I/Q) processing, and the dual unipolar signal with wavelength tagging and a bipolar LO with I/Q processing. Examples of resulting power spectra from the simulated signals plus noise are shown and discussed for some selected cases, but the SNR results from the simulations for these various configurations and their comparison with the theory are shown and discussed in section 4.

The Monte Carlo simulations use the rnbinom and rpois functions in Mathcad® to generate the negative binomial distributed signal counts and Poisson distributed noise counts, respectively, in accordance with the theory of Gatt, et. al.. [ref 26]

The signal, LO, and noise models and some selected simulation power spectra results using the rnbinom and rpois functions with their arguments are shown below first for the unipolar signal and unipolar DLLO without I/Q demodulation case, followed by a discussion of simulation modifications for the subsequent cases of a bipolar DLLO, a bipolar DLLO with I/Q demodulation, and a dual unipolar signal and bipolar DLLO with I/Q demodulation.

Note that since the simulated data are quantized to one bit, the single-bit quantization noise is inherently included in the simulated power spectra.

The Monte Carlo simulations generate 24 to 64 realizations of signal plus noise for an up-chirp AM signal waveform. The simulations were run for the following parameter values:

N_{trials} = Number of simulation trials = 24-64 N_s = Number of samples = 2^{13}

Δt = Sample duration = 0.5 ns = dead-time t_{chirp} = chirp duration = 4.096 μs

f_0 = 100 MHz = chirp start frequency f_s = 500 MHz = chirp stop frequency

Target Range = 2.99963379 m Target IF = 1.953125 MHz

M = speckle diversity = 1 or 1E+06

counts_noise_td = mean number of additive noise counts per sample time set equal to the dead-time = about 1E-04 for unipolar signal or 2E-04 for dual unipolar signal with wavelength tagging

counts_signal_td = mean number of signal counts per sample time = from about 0.05 to 1

counts_total_td = mean number of total counts per sample time
= counts_noise_td + counts_signal_td = from about 0.05 to 1

Note that the value of the target range used in the simulations is chosen so that the resulting round-trip delay time makes the intermediate frequency (IF) for the target return signal exactly equal to some frequency sample in the power spectrum computed in the simulations to avoid

complications in computing the SNR for comparison to the theory due to the target range peak straddling two frequency samples.

For the number of samples accumulated of 2^{13} used in the simulations, the mean total number of noise counts accumulated over the chirp duration of 4.096 μs in the simulations is about 0.8192, corresponding to an average noise count rate of about 200 kHz for counts_noise_td = 1E-4. Since the dual unipolar signal with wavelength tagging receiver uses two Gm-APDs from which the signals and noise are added, counts_noise_td = 2E-4 for this case, i.e., 1E-4 from each of the two Gm-APD detectors.

The number of simulation trials used for each case are given in the appropriate subsections below describing the simulations.

3.1. Unipolar Signal and Unipolar DLLO Simulation Description and Power Spectra Results

The signal, LO, and noise models with the rnbinom and rpois functions with their arguments for the unipolar signal and unipolar DLLO without I/Q demodulation are shown below.

$$signal_i := 0.5\cdot\left[1 + \sin\left[2\cdot\pi\cdot\left[f_0 + k_f\cdot\left(t_i - \frac{2\cdot R_{tgt}}{c} - \tau_{txdelay}\right)\right]\cdot t_i\right]\right] \quad \text{for a sinusoidal waveform (15. a.)}$$

$$signal_i := 0.5\cdot\left[1 + sign\left[\sin\left[2\cdot\pi\cdot\left[f_0 + k_f\cdot\left(t_i - \frac{2\cdot R_{tgt}}{c} - \tau_{txdelay}\right)\right]\cdot t_i\right]\right]\right] \quad \text{for a square waveform (15. b.)}$$

$$LO_i := 0.5\cdot\left[1 + sign\left[\sin\left[2\pi\cdot\left(f_0 + k_f\cdot t_i\right)\cdot t_i\right]\right]\right] \quad \text{for a square wave LO} \quad (16.)$$

where f_0 = the start frequency of the chirp
k_f = the temporal slope of the chirp = $(f_s - f_0)/T_{chirp}$, where f_s = the stop frequency of the chirp, and T_{chirp} = the duration of the chirp
t_i = the i^{th} sample time from the start of the chirp
R_{tgt} = the target range for the simulations
c = $3 \cdot 10^8$ in m/s, the speed of light in vacuum.
$\tau_{txdelay}$ = an additional delay added to the transmitted waveform to move the harmonics beyond the IF of the desired unambiguous range.
sign[] = the sign of the argument function, which returns +1 for a non-negative number for the argument and -1 for a negative number for the argument.

The random Poisson distributed noise counts and negative binomial distributed signal counts per sample time are given by equations (17.) and (18.), respectively:

$$counts\_n\_rnd_{i,j} := if(rpois(Ntrials, m\_n_i)_j > 0,1,0) \quad (17.)$$

$$counts\_s\_rnd_{i,j} := if[(rnbinom(N_{trials}, M, p_i)_j > 0) \text{ ^ } (counts\_n\_rnd_{i,j} = 0),1,0] \quad (18.)$$

where In Mathcad®, the function if(logical expression, A, B) means that if the logical

expression is true, then the result is A, otherwise the result is B
In Mathcad®, the symbol ^ represents the Boolean logical AND
i = row index over sample times
j = column index over trials

Note: The "if" statements in equations (17.) and (18.) enforce the restriction of having at most one count output by the Gm-APD per dead-time, which equals the clock time interval in the simulations.

In Mathcad®, rnbinom(m,n,p) returns a vector of m random numbers having the negative binomial distribution:

Negative binomial

$$\binom{n+k-1}{k}\cdot p^{n}\cdot(1-p)^{k}$$

in which $0<p\leq 1$ and n and k are integers, $n>0$ and $k\geq 0$. (19.)

where for the Gamma Poisson (mixture) parameterization used by Gatt, et. al., we have

$m = N_{trials}$ = the number of trials in the simulations

$n = M$ = the speckle diversity

$$p_i := \frac{M}{M + m\_s_i} \qquad (20.)$$

where m_s_i = the mean number of signal photoelectrons in the i^{th} sample time in the simulations prior to applying the limit of 1 count output by the Gm-APD per dead-time, which equals the sample duration in the simulations.

$= A_s \cdot signal_i$, where A_s is the user input signal amplitude factor which is varied to change the number of signal photoelectrons and counts in the simulations.

In Mathcad®, rpois(m,λ) returns a vector of m random numbers having the Poisson distribution:

Poisson

$$\frac{\lambda^{k}}{k!}\cdot e^{-\lambda}$$

in which $\lambda>0$ and k is a non-negative integer. (21.)

where $m = N_{trials}$ = the number of trials in the simulations

$\lambda = m\_n_i$ = the mean number of noise photoelectrons in the i^{th} sample time in the simulations prior to applying the limit of 1 count output by the Gm-APD per dead-time, which equals the sample duration in the simulations.

The following expression in Mathcad® performs the logical AND on the single-bit signal plus

noise counts and the single-bit LO data streams to produce the single-bit mixer output:

$$\text{Mixed}^{\langle j \rangle} := \overrightarrow{(\text{counts\_tot\_rnd}^{\langle j \rangle} \wedge \text{LO})} \quad (22.)$$

where $\text{counts\_tot\_rnd}^{\langle j \rangle} := \overrightarrow{(\text{counts\_s\_rnd}^{\langle j \rangle} + \text{counts\_n\_rnd}^{\langle j \rangle})}$

= the j^{th} column vector of random total signal plus noise counts at every sample time for the j^{th} trial

j = column index over trials, and the superscript <j> indicates the j^{th} column of a 2D array.

The single-bit mixer output is Hann windowed to reduce sidelobes, and zero padded to eight times its original length. The Hann window is given by

$$w_{hann_i} := \sin\left(\frac{\pi \cdot i}{N_s - 1}\right)^2 \quad (23.)$$

The Hann windowed and zero padded single-bit mixer output is digitally bandpass filtered by a super Gaussian filter that filters out the DC peak and high frequencies prior to down sampling to prevent aliasing. The digital super Gaussian band pass filter for the zero padded signal is defined in the frequency domain by the following in the Mathcad® simulations:

$$SGBPF_{ii} := \text{if}\left[ii \le \text{ceil}\left(\frac{N_s \cdot 8}{2}\right), \exp\left[\frac{-ii^{50}}{(121 \cdot 8)^{50}}\right], \exp\left[\frac{-(ii - N_s + 1)^{50}}{(121 \cdot 8)^{50}}\right]\right]$$

$$SGBPF_0 := 0$$

$$SGBPF_1 := 0$$

$$SGBPF_{8 \cdot N_s - 1} := 0 \quad (24.)$$

where ceil() = the round up to the next highest integer function

ii = index over the frequency bins

Figure 7 is a graph of the frequency response of the super Gaussian band pass filter used in the simulations as defined by equation (24.). The filter's upper cut-off frequency is set just below one-half the simulation's 2 GHz clock rate divided by 32, which equals 31.25 MHz, for anti-aliasing when down sampling by a factor of 32.

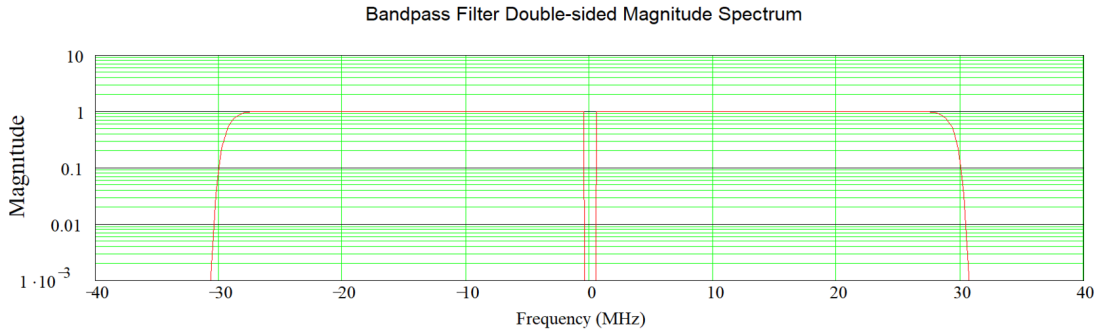

Figure 7. Super Gaussian band pass filter frequency response.

The super Gaussian band pass filter function is multiplied by the complex fast Fourier transform

(cfft) of the Hann windowed and zero padded single-bit mixer output. The real part of the inverse cfft (icfft) of the resulting product is the filtered mixer output which is then down sampled by a factor of 32 as follows:

$$iv := 0 .. 8 \cdot \frac{N_s}{32} - 1$$

$$Mixed\_filt\_ds_{iv,j} := \sum_{n=0}^{32-1} Mixed\_filt_{32 \cdot iv + n, j} \qquad (25.)$$

where Mixed_filt_ds = the filtered and down sampled Hann windowed and zero padded mixer output

Mixed_filt = the filtered Hann windowed and zero padded mixer output prior to down sampling

The power spectrum of the filtered and down sampled Hann windowed and zero padded single-bit mixer output is computed in Mathcad® for each trial. The resulting power spectra are averaged together to produce the mean power spectrum for all the trials.

The mean noise floor of this mean power spectrum is computed over the portion of the spectrum between the target signal's fundamental IF and the third harmonic of that frequency. The value of this mean noise floor is the denominator in computing a simulation's mean SNR. The peak value of the mean power spectrum at the fundamental IF minus the value of the mean noise floor is used as the numerator in computing a simulation's mean SNR.

Figure 8 shows the mean power spectrum of the Hann windowed and zero padded single-bit mixer output after band pass filtering and down sampling by a factor of 32, for each of low and high signal levels from the simulations for a chirped sinusoidal signal.

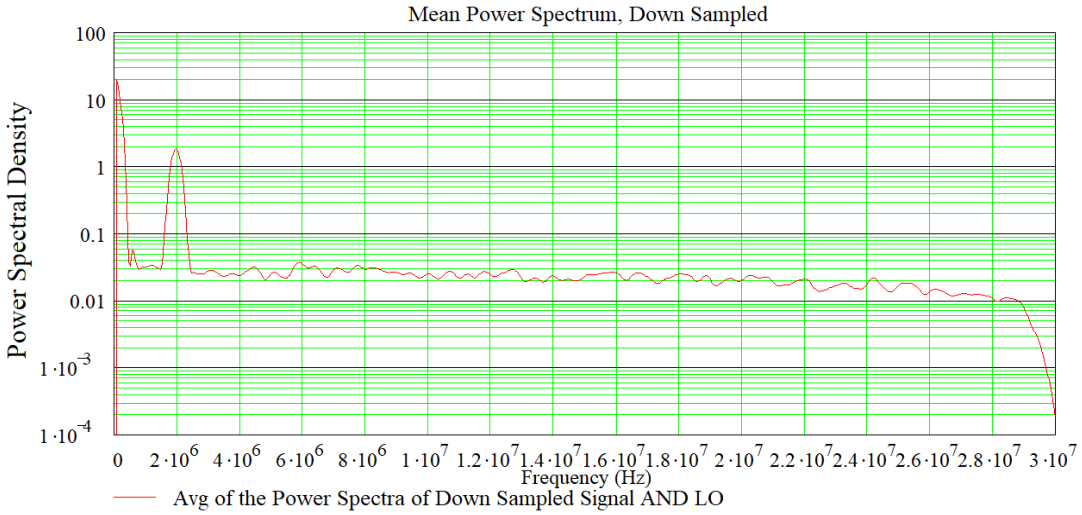

(a.) Low mean counts per dead-time (counts_tot_td = 0.2) - chirped sinusoidal signal

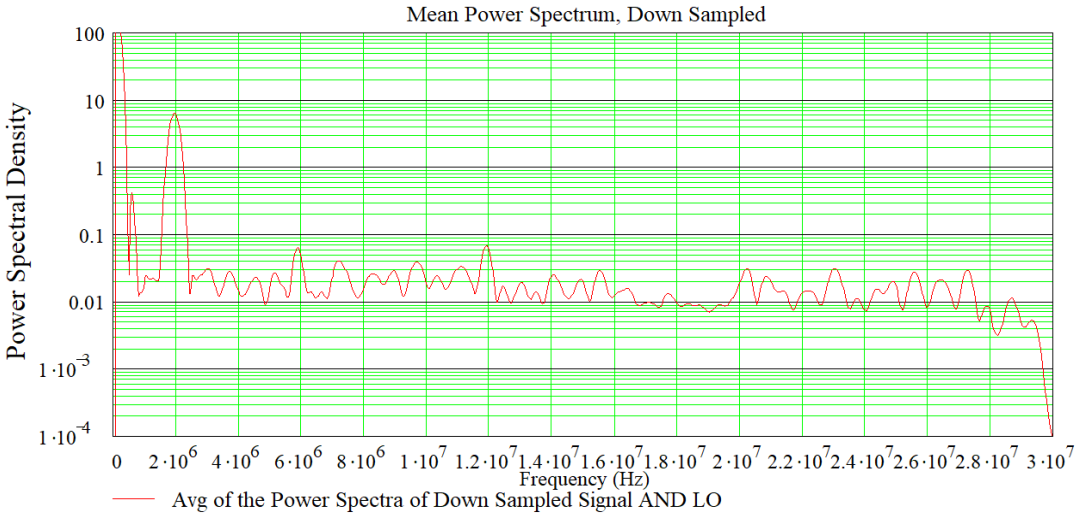

(b.) High mean counts per sample time (counts_tot_td = 0.8) - chirped sinusoidal signal

Figure 8. Mean filtered and down sampled signal AND LO plus noise power spectrum from the Mathcad® Monte Carlo simulations for a chirped sinusoidal signal with counts_n_td = 1E-04 and M=1E+06 for each of low and high signal levels (a.) Low mean counts per dead-time (counts_tot_td = 0.2) and (b.) High mean counts per dead-time (counts_tot_td = 0.8).

Figure 9 shows the mean power spectrum of the Hann windowed and zero padded single-bit mixer output after band pass filtering and down sampling by a factor of 32, for each of low and high signal levels from the simulations for a chirped square wave signal.

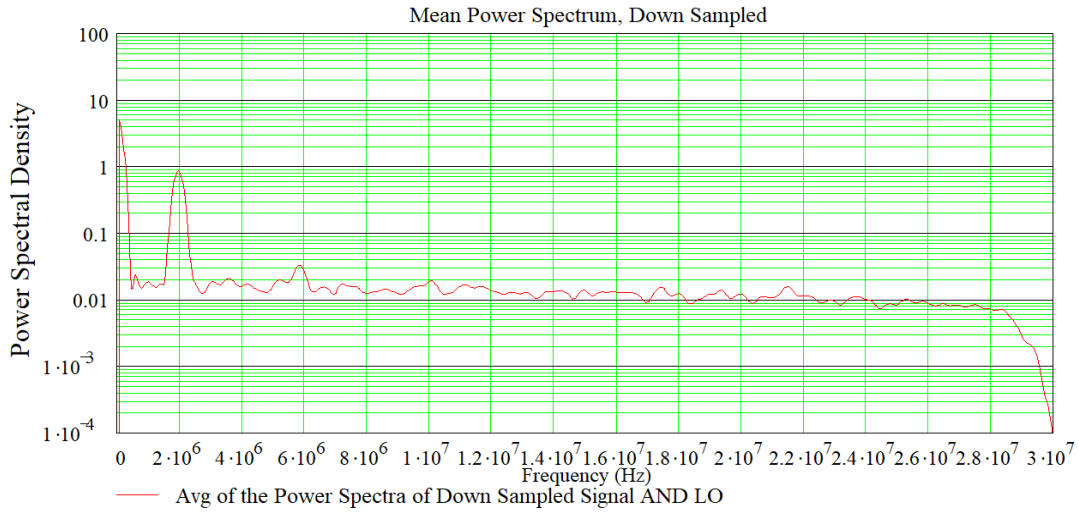

(a.) Low mean counts per sample time (counts_tot_td = 0.2) - chirped square wave signal

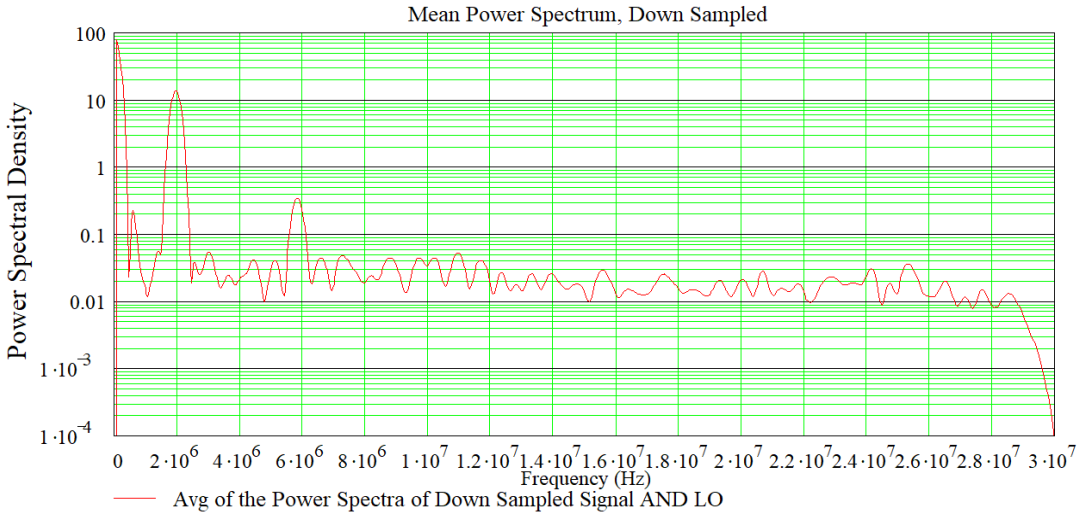

(b.) High mean counts per sample time (counts_tot_td = 0.8) - chirped square wave signal

Figure 9. Mean filtered and down sampled signal AND LO plus noise power spectrum from the Mathcad® Monte Carlo simulations for a chirped square wave signal with counts_n_td = 1E-04 and M=1E+06 for each of low and high signal levels (a.) Low mean counts per dead-time (counts_tot_td = 0.2) and (b.) High signal counts per sample time (counts_tot_td = 0.8).

As explained in section 2.1, for the fully modulated chirped square wave signal the samples where the zeroes of the chirped square wave are located are never filled by 1's for any signal level, and those samples can only have an occasional 1 due to noise at the low noise levels in the simulations and in a well designed PC-CAML. Therefore, as counts_tot_td approaches 1, only the samples corresponding to the high levels of the chirped square wave become filled with 1's, and this causes the waveform to approach the uniformly sampled deterministic chirped square wave form as counts_tot_td approaches 1. This results in the floor of the power spectrum of the chirped square wave signal plus noise becoming dominated by sidelobes and perhaps aliasing, depending on the signal bandwidth and clock rate, as counts_tot_td approaches 1.

This is illustrated by the graph in figure 10 of the raw power spectra prior to filtering and down sampling for the simulated PC-CAML's stochastic chirped square wave signal for counts_tot_td = 1, counts_n_td = 1E-4, and M = 1E+06 ANDed with a deterministic chirped square wave LO (red trace), and a noiseless, deterministic chirped square wave signal multiplied by a deterministic chirped square wave LO (blue trace).

Clearly, the power spectrum, including the floor between the spectral peaks, for the mixer outputs with the stochastic chirped square wave signal for counts_tot_td = 1 ANDed with the chirped square wave LO is nearly identical to that of the noiseless, deterministic chirped square wave signal times the chirped square wave LO.

Note that a well designed PC-CAML system using transmitter power and/or receiver throughput control to prevent saturation would operate at the lower signal levels where the spectral floor is dominated by noise.

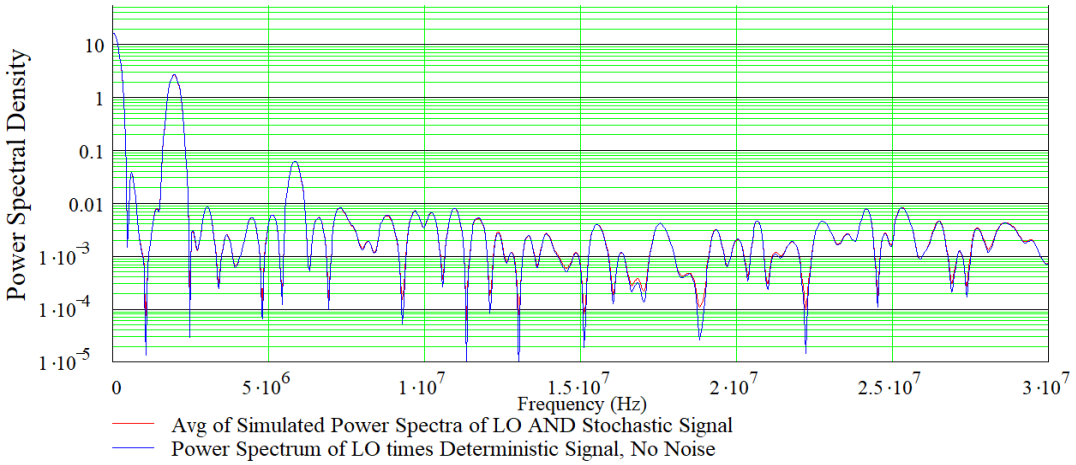

Figure 10. Comparison of simulated raw power spectra prior to filtering and down sampling of the chirped square wave LO ANDed with the stochastic chirped square wave signal for counts_tot_td = 1, counts_n_td = 1E-4, and M = 1E+06 (red trace) versus the chirped square wave LO multiplied by the noiseless, deterministic chirped square wave signal (blue trace).

3.1.1. Simulation Results for the Transmitted Waveform Delay to Shift the Harmonics

Figure 11 shows the mean power spectrum without (a.) and with (b.) an additional 59.99 ns delay on the transmitted chirped square wave signal. In the latter case, the frequencies plotted have all been digitally shifted by subtracting the intermediate frequency (IF) corresponding to the additional transmitted waveform delay to return the fundamental IF peak corresponding to the target range to its original position without the additional delay. These simulation results demonstrate the ability of the additional delay on the transmitted waveform to move the harmonics beyond the desired unambiguous range. This technique works because adding a delay to the transmitted waveform spreads the frequency difference between the fundamental IF and its n^{th} harmonic since the n^{th} harmonic has n times the chirp bandwidth making its frequency slope over the same waveform duration n times steeper. (See ref 18, pp. 11-12, and ref 17, section 3.1 for more details on this technique.)

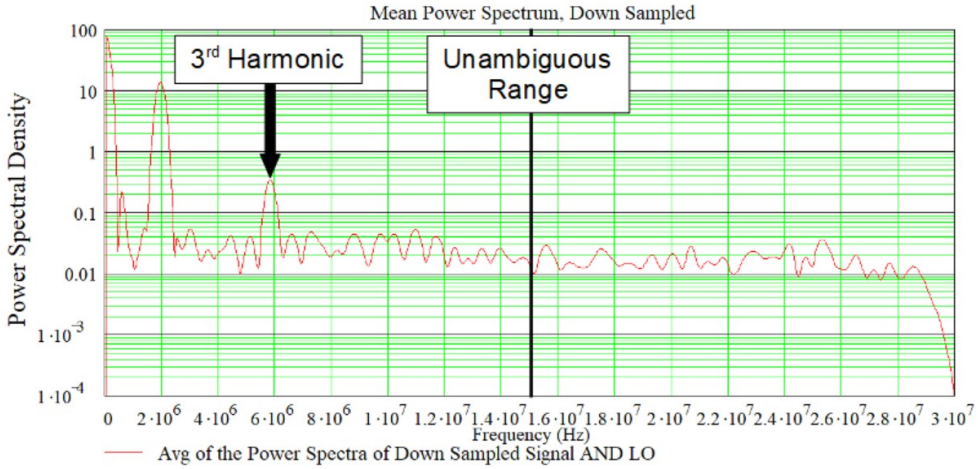

(a.) No additional Delay on the Transmitted Waveform

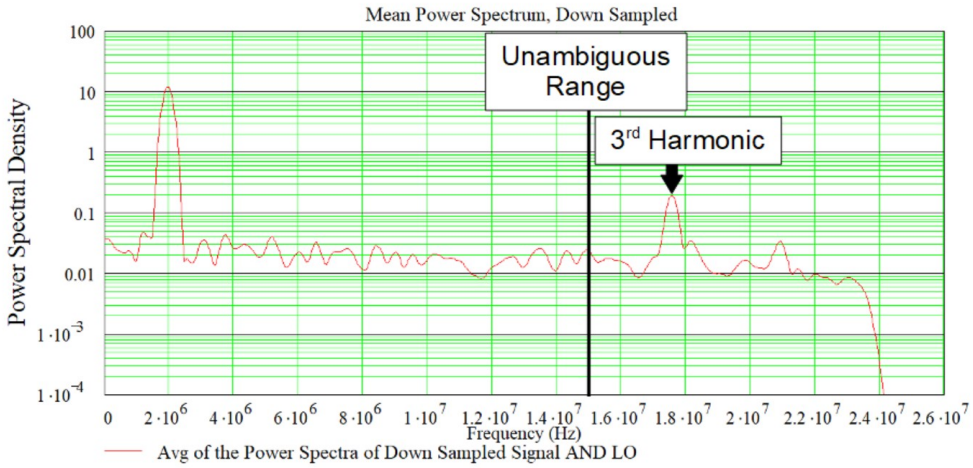

(b.) With an additional Delay of 59.99 ns on the Transmitted Waveform

Figure 11. Power Spectrum without (a.) and with (b.) an additional delay of 59.99 ns on the transmitted chirped square wave signal, with counts_tot_td = 0.8, counts_n_td = 1E-04, and M = 1E+06.

Bjorndal points out that in addition to the harmonics, there will also be a number of cross-products, so care must be taken such that the cross terms are also easy to filter out. [ref 18, p. 12.] As Bjorndal, et. al., note "If the desired unambiguous range is large, the above approach may necessitate an impractically long delay." [ref 17]. In this case, Bjorndal, et. al., provide alternative methods for dealing with the harmonics as detailed in references 17 and 18.

3.2. Modifications for a Unipolar Signal and a Bipolar DLLO

The only changes for the unipolar signal and bipolar DLLO simulations compared to those in the previous section are as follows:

1. Simulating only a chirped sinusoidal signal instead of both a chirped sinusoidal signal and a chirped square wave signal
2. Using the sign of a bipolar chirped square wave LO (equation (26.) below) instead of the unipolar chirped square wave LO
3. Using the power spectrum of the IF signal without filtering and down sampling as used in the previous section since the SNR does not differ significantly before and after filtering and down sampling
4. Implementing looping over the average number of signal counts per sample time requiring storing the results in 3D arrays instead of 2D arrays so that the SNR plots were generated by running the Mathcad® worksheet once instead of multiple times with the value of the average number of signal counts per sample time being changed manually for each run as done previously. This change required reducing the number of trials in the simulations to 24 from the 64 trials used in the previous section since the 3D data arrays are much larger in the current simulations and required too much memory for more than 24 trials. The results with 24 trials in the simulations indicate that 24 trials are sufficient, and the results are generated much faster. Therefore, 24 trials were used for the simulations of all the remaining configurations.

The equation for the sign of the bipolar chirped square wave DLLO is given by

$$LO := \overrightarrow{sign\left[\sin\left[2\pi\cdot\left(f_0 + k_f\cdot t\right)\cdot t\right]\right]} \quad (26.)$$

where f_0 = the start frequency of the chirp
k_f = the temporal slope of the chirp = $(f_s - f_0)/T_{chirp}$, where f_s = the stop frequency of the chirp, and T_{chirp} = the duration of the chirp
t = the clock time from the start of the chirp
sign[] = the sign of the argument.

In the simulations, the LO's sign is applied to the signal's value by multiplying the result of equation (26.) and the signal value for each sample.

The Monte Carlo simulations generate 24 realizations of signal plus noise for an up-chirp AM signal waveform.

3.3. Modifications for a Unipolar Signal and a Bipolar DLLO with I/Q Demodulation

The only changes for the unipolar signal and bipolar DLLO with digital I/Q demodulation simulations compared to those in the previous section are as follows:

1. Using the sign of a bipolar chirped cosine (in-phase (I)) square wave DLLO (equation (27 a.)) and the sign of a bipolar chirped sine (quadrature-phase (Q)) square wave DLLO (equation (27 b.)) instead of the sign of the single bipolar chirped square wave DLLO used in section 3.2
2. Forming the complex analytic signal from the outputs of the I and Q digital mixers, and computing the power spectra of this complex analytic signal plus noise for 24 trials in the Monte Carlo simulations.

The equations for the sign of the I and Q bipolar chirped square wave DLLOs are given by

$$LO\_I := \overrightarrow{sign\left[\cos\left[2\pi\cdot\left(f_0 + k_f\cdot t\right)\cdot t\right]\right]} \quad (27\text{ a.})$$

$$LO\_Q := \overrightarrow{sign\left[\sin\left[2\pi\cdot\left(f_0 + k_f\cdot t\right)\cdot t\right]\right]} \quad (27\text{ b.})$$

where f_0 = the start frequency of the chirp
k_f = the temporal slope of the chirp = $(f_s - f_0)/T_{chirp}$, where f_s = the stop frequency of the chirp, and T_{chirp} = the duration of the chirp
t = the clock time from the start of the chirp
sign[] = the sign of the argument.

In the simulations, the LOs' signs are applied to the signal's value by multiplying separately the results of equations (27 a.) and (27 b.) by the signal value for each sample to form the digitally mixed I and Q intermediate frequency (IF) signals. The I and Q IF signals are combined as follows to form the complex analytic signal:

IQ_cplx = Mixed_I – i Mixed_Q (28.)

where Mixed_I = the product of LO_I and the signal plus noise counts

Mixed_Q = the product of the LO_Q and the signal plus noise counts

$i = (-1)^{1/2}$

The complex analytic signal is Hann windowed to reduce sidelobes in the IF power spectrum. The Hann windowed complex analytic signal is zero padded to eight times the original length. The power spectrum of the Hann windowed and zero padded complex analytic signal is computed in Mathcad® for each trial. The resulting power spectra are averaged together to produce the mean power spectrum for all the trials.

The mean noise floor of this mean power spectrum is computed over the portion of the spectrum between the target signal's fundamental IF and the third harmonic of that frequency. The value of this mean noise floor is the denominator in computing a simulation's mean SNR. The peak value of the mean power spectrum at the fundamental IF minus the value of the mean noise floor is used as the numerator in computing a simulation's mean SNR.

The Monte Carlo simulations generate 24 realizations of signal plus noise for an up-chirp AM signal waveform.

3.4. Modifications for a Dual-Unipolar Signal and a Bipolar DLLO with I/Q Demodulation

The only changes for the dual unipolar signal with bipolar DLLOs and digital I/Q demodulation simulations compared to those in the previous section are as follows:

1. Using the dual unipolar signal equations shown in equations (29 b.) and (29 c.) below, derived from the bipolar chirped sinusoidal signal shown in equation (29 a.) below.
2. Using zero padding to 4 times the original signal length instead of 8 times the original signal length as used in the previous sections since 8 times zero padding caused memory problems in generating and processing two unipolar signals in the dual unipolar signal case that had not occurred for the one unipolar signal used in the previous sections. Note that the 4 times zero padding was sufficient to provide good results.
3. The value of the mean number of additive noise counts per dead-time, counts_n_td, is twice the value used in the simulations for the unipolar signals presented in the previous sections due to the use of two Gm-APD detectors in the wavelength tagging version of the dual unipolar bitstream PC-CAML receiver architecture shown in figure 5 (b.). Each Gm-APD has the same value of the mean number of additive noise counts per sample time as used for the single Gm-APD receiver simulated in the previous sections.

The equations for the bipolar chirped sinusoidal signal and the two unipolar chirped sinusoidal signals derived from it are given by

$$\overrightarrow{\text{signal} := \sin\left[2\cdot\pi\cdot\left[f_0 + k_f\cdot\left(t - \frac{2\cdot R_{tgt}}{c} - \tau_{txdelay}\right)\right]\cdot t\right]} \quad (29\text{ a.})$$

$$signal1_i := if(signal_i > 0, signal_i, 0) \quad (29\ b.)$$

$$signal2_i := if(signal_i < 0, -signal_i, 0) \quad (29\ c.)$$

where f_0 = the start frequency of the chirp
k_f = the temporal slope of the chirp = $(f_s - f_0)/T_{chirp}$, where f_s = the stop frequency of the chirp, and T_{chirp} = the duration of the chirp
t = the clock time from the start of the chirp
i = index over sample times
if(*arg1, arg2, arg3*) = *arg2* if *arg1* is true; *arg3*, otherwise.

In the simulations, the mean number of signal photoelectrons in a sample prior to applying the dead-time restrictions on the detected counts is modulated by each of the signals resulting from equations (29 b.) and (29 c.) for input to the negative binomial random number generator for each channel of the dual unipolar signal in the same way as for the single unipolar signal as detailed in the previous sections.

Each of the unipolar signals' random realizations are then subjected to the restriction of the Gm-APD's output having at most a single signal plus noise count per dead-time which is set equal to the sample time in the simulations, in the same way as detailed for the single unipolar signal in previous sections. The resulting single-bit unipolar random signal plus noise count data stream for each channel is then processed and combined into a single bipolar random signal plus noise signed binary digital data stream as indicated in figure 5 (b.).

The bipolar signal plus noise binary digital data stream is duplicated with one copy being multiplied by the bipolar chirped cosine DLLO signed binary digital data for the in-phase (I) channel, and the other copy being multiplied by the bipolar chirped sine DLLO signed binary digital data for the quadrature-phase (Q) channel to form the digitally mixed I and Q intermediate frequency (IF) signals plus noise in accordance with figure 5 (b.). The I and Q IF signals are combined as follows to form the complex analytic signal:

$$IQ\_cplx = Mixed\_I - i\ Mixed\_Q \quad (30.)$$

where Mixed_I = the I bipolar DLLO times the bipolar signal plus noise data
Mixed_Q = the Q bipolar DLLO times the bipolar signal plus noise data
$i = (-1)^{1/2}$

The complex analytic signal is Hann windowed to reduce sidelobes in the IF power spectrum. The Hann windowed complex analytic signal is zero padded to four times the original length. The power spectrum of the Hann windowed and zero padded complex analytic signal is computed in Mathcad® for each trial. The resulting power spectra are averaged together to produce the mean power spectrum for all the trials.

The mean noise floor of this mean power spectrum is computed over the portion of the spectrum between the target signal's fundamental IF and the fifth harmonic of that frequency since this is the first higher harmonic visible in the IF spectrum of the dual unipolar signal as it squares off at higher signal levels due to Gm-APD saturation. The value of this mean noise floor is the

denominator in computing a simulation's mean SNR. The peak value of the mean power spectrum at the fundamental IF minus the value of the mean noise floor is used as the numerator in computing a simulation's mean SNR.

4. Simulation and Theory SNR Results Comparison

As shown by the simulation and theoretical results summarized in figures 12 and 13, the SNR improves at each step in going from the original bitstream PC-CAML in its simplest implementation with a unipolar chirped AM sinusoidal signal and a single channel unipolar DLLO, to a unipolar chirped AM sinusoidal signal and a single channel bipolar DLLO, to unipolar chirped AM sinusoidal signal and bipolar DLLOs with digital I/Q demodulation, and finally to a dual unipolar chirped AM sinusoidal signal and bipolar DLLOs with digital I/Q demodulation, with increasing system complexity at each step. Whether or not this additional complexity is worth the improved SNR will have to be decided from system trade studies.

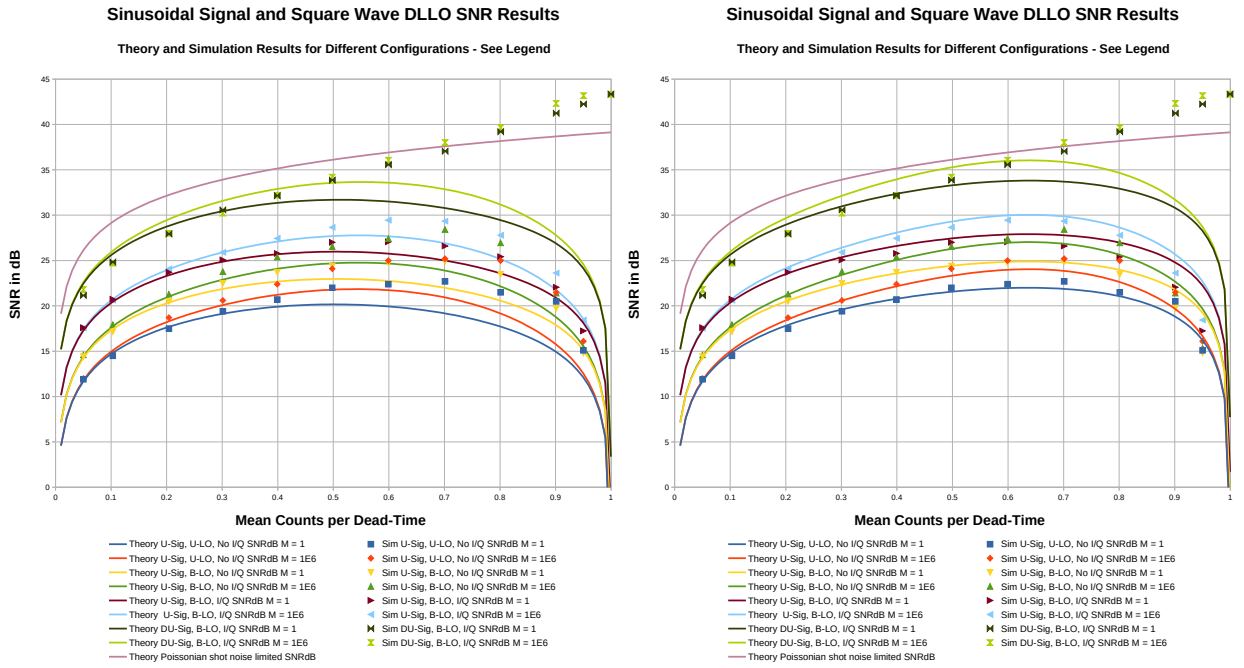

(a.) (b.)

Figure 12. Comparisons of SNR results from the Monte Carlo simulations and SNR theory for different bitstream PC-CAML configurations with a chirped sinusoidal signal and square wave DLLO as a function of mean total counts per deadtime. (a.) SNR in dB from the simulations and from the SNR theory with the original steady state arm probability, and (b.) SNR in dB from the simulations and from the SNR theory with the modified steady state arm probability.

Figure 12 also shows that in the simulation results, the Dual Unipolar chirped sinusoidal signal and chirped square wave Bipolar DLLO with digital I/Q demodulation achieves about the same SNR as that for Poissonian shot noise limited operation for a mean total counts per dead-time of about 0.7, corresponding to 5734 mean counts accumulated. At mean total counts per dead-time less than this, the Hann window loss, dark noise and quantization noise reduce the SNR to less than that of the shot noise limited case. At mean total counts per dead-time greater than about 0.7

where the signal level is in the saturation regime, the SNR from the simulation results exceeds that of the shot noise limited case because saturation suppresses the fluctuations due to noise, including the fluctuations due to shot noise. In addition, the theoretical SNR for this case for mean total counts per dead-time greater than about 0.7, rolls off due to the reduction in arm probability whereas the simulation results SNR continues to increase as each wavelength channel's signal becomes closer to a noiseless chirped square wave as discussed in section 2.1. These phenomena seen in the simulation results but not in the SNR theory results should be investigated in future work.

The simulation results for the unipolar chirped sinusoidal signal with a unipolar chirped square wave DLLO without I/Q processing (U-Sig, U-LO, No I/Q cases) and the SNR theory using the original steady-state arm probability are in good agreement up to a mean total counts per dead-time of about 0.3 for both M=1 and M=1E+06. Using the SNR theory with the modified steady-state arm probability provides good agreement up to a mean total counts per dead-time of about 0.5 for both M=1 and M=1E+06. Above these levels, both SNR theories under predict the simulation results, but using the modified arm probability fits the simulation results better, especially for the M=1 case. For the mean total counts per dead-time regime of 0.05 to 0.5, the theory and simulation results predict SNRs of about 10-23 dB for the additive noise level of counts_n_td = 1E-4. Note that a well designed PC-CAML system using transmitter power and/or receiver throughput control to prevent saturation would operate at these lower signal levels where the initial SNR theory agrees with the simulation results, and where the spectral floor is dominated by noise.

Also, note that prior to adding the quantization noise term, the SNR theory over estimated the SNR compared to the simulation results for low counts_tot_td (less than about 0.2), but after addition of the quantization noise terms, the SNR theory is in good agreement with the simulation results for these low values of counts_tot_td. Thus, it is important to account for the quantization noise caused by the single-bit quantization inherent in the bitstream PC-CAML in the theory. This also indicates that the single-bit quantization noise is inherently built into the simulations since the received signals and the DLLO are single-bit (i.e., having 2 discrete levels).

Considering the simulation and SNR theory (with modified arm probability) results in figures 12 and 13, for the unipolar signals with bipolar DLLO with digital I/Q demodulation cases (U-Sig B-LO, I/Q cases), at the lower signal levels corresponding to mean total counts per dead time of about 0.4 and lower, the SNRs are about 5 dB to 6 dB higher than those for the unipolar DLLO with a single channel of digital mixing. These SNR results for the unipolar signal and bipolar DLLO with digital I/Q demodulation are also about 2 dB to 3 dB higher than those for the unipolar signal and bipolar DLLO with a single channel of digital mixing as shown in figures 12 and 13.

The simulation results and the theory for the dual unipolar signal are qualitatively different in that the simulation results for M = 1 and M = 1E+06 do not differ significantly even for higher signal levels as they do for the SNR Theory results. See the earlier discussion of a tentative conjecture to explain this in section 2.2.

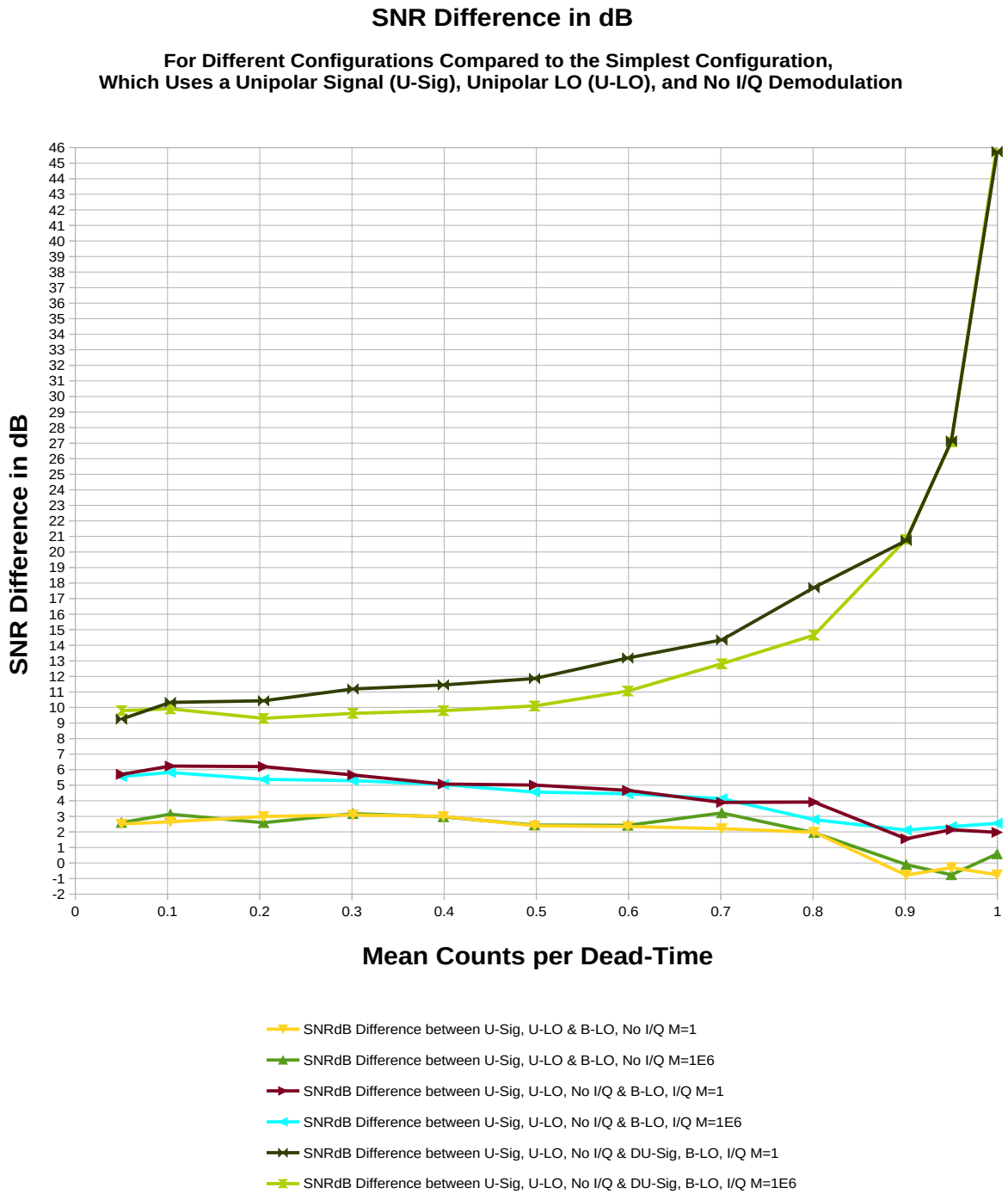

Figure 13. Difference in dB of the simulations SNR results for each configuration compared to the simplest configuration using a unipolar signal (U-Sig), unipolar LO (U-LO), and no I/Q demodulation versus mean counts per dead-time.

In addition, at counts_tot_td above about 0.7, the SNR values for the dual unipolar chirped sinusoidal signal simulation results exceed those of the shot noise limited theoretical curve and continue to increase, whereas the theoretical SNR values rollover to approach zero as

counts_tot_td approaches 1. The simulation results, however, indicate that for the unipolar square wave modulated chirp signal and the dual unipolar sinusoidally modulated chirp signal, the SNR does not roll-off in the saturation regime. This paper explains why this may be in section 2.1.

Note that Gatt, et. al. state "An expression for the SNR is developed in Subsection 4.B, where it is shown that, in the high signal limit, the SNR can exceed the Poisson or quantum limit. This is due to nonlinear saturation or bleaching effects that result in reduced signal variance."[ref 26, p.3263] They also state “It is shown that SNR is not necessarily a useful metric for GM-APD devices since, when in saturation, the GM-APD SNR can exceed the Poisson quantum limit due to reduced signal variance”[ref 26, p.3268] and “SNRs in excess of the Poissonian GM-APD output theory are an indication that the device is behaving nonlinearly and less information (e.g., target reflectance) is available due to saturation.”[ref 26, p.3271]

The missing information due to saturation (e.g., target reflectance), however, is not needed for some applications, so for those applications, the higher than quantum limited SNR is useful for improving the quality of the information that can be collected such as target range and velocity. The simulation results for the unipolar square wave modulated and dual unipolar sinusoidally modulated chirp signals with a bipolar square wave chirp DLLO and I/Q demodulation showed this effect of exceeding the Poisson quantum limited SNR in the high signal limit, so those waveforms may be very well suited for applications for which target reflectance data is not needed and for which there may be large signal amplitude variations that would be suppressed by operating in the Gm-APD’s saturation regime.

Usually, however, a well designed PC-CAML system using transmitter power and/or receiver throughput control to prevent saturation would operate at signal levels below the onset of saturation where the initial SNR theory is at or above the simulation results, i.e, for counts_tot_td values of about 0.5 or less. For these signal levels, these SNR results for the dual unipolar signal and bipolar DLLOs with digital I/Q demodulation are also from about 3.5 dB to about 7 dB higher than those for the unipolar chirped sinusoidal signal and bipolar DLLOs with digital I/Q demodulation as shown in figures 12 and 13.

The SNR improvement at the very low signal levels (less than about 0.3 mean total counts per dead-time) is less than the 6 dB SNR improvement expected for a bipolar signal over that of a unipolar signal because of the higher additive noise due to using two Gm-APDs instead one Gm-APD and due to the higher quantization noise for the dual unipolar signal as explained above. The additive noise is larger relative to the signal shot noise at the lower signal levels so that it has a larger effect on reducing the SNR improvement at lower signal levels.

On the other hand, if the signal levels are allowed to approach Gm-APD saturation, the fully modulated dual unipolar signal bitstream PC-CAML shows an SNR improvement that is larger than 6 dB at higher signal levels approaching saturation due to its continued increase in SNR with higher signal levels approaching saturation compared to the decreasing SNR with higher signal levels approaching saturation for the unipolar chirped sinusoidal signal bitstream PC-CAML. The unipolar chirped sinusoidal signal with a bipolar DLLO and digital I/Q demodulation bitstream PC-CAML’s simulated SNR shown in figure 12 peaks at about 27 dB for M=1 and at about 29.5 dB for M=1E6, for counts_tot_td between 0.6 and 0.7, whereas the dual

unipolar signal with a bipolar DLLO and digital I/Q demodulation PC-CAML reaches a maximum simulated SNR of about 43 dB for counts_tot_td of 1, and is about 37 dB for counts_tot_td between 0.6 and 0.7.

5. Initial Proof-of-Concept Experiment

An initial proof-of-concept experiment for the bitstream PC-CAML with a DLLO was performed for the chirped unipolar sinusoidal waveform using the setup shown in figure 14. In this setup, the mini-PC streams the sinusoidal chirp digital data from a .wav file to the Oppo UDP-203 player which converts the digital data to an analog audio line level output electrical signal, which is input into an audio amplifier. The headphone amplifier outputs the amplified analog chirp signal from its speaker outputs to the input of a modulatable white light LED flashlight designed to modulate the optical power output by the LED at frequencies within the audio band.

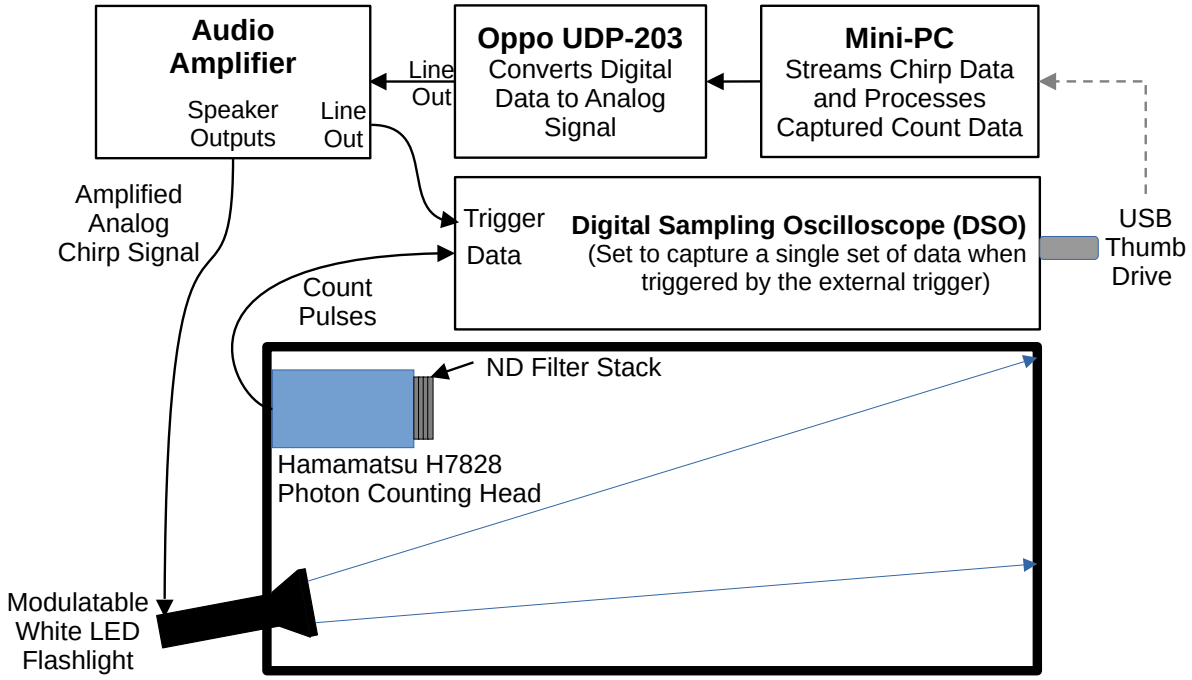

Figure 14. Bitstream PC-CAML with a DLLO first experimental setup diagram.

The audio amplifier also outputs the audio line level signal to the external trigger input of a digital sampling oscilloscope (DSO). The data file containing the chirp signal also contains a trigger pulse signal which precedes the start of the chirp signal. The DSO is set to start the capture of a single dataset on the falling edge of the trigger pulse which occurs about 95.13 ms prior to the start of the 185.8 ms duration chirp signal in order to account for the 95.03 ms delay from the trigger to the start of the data capture in the DSO, so that the data capture starts 0.1 ms prior to the start of the chirp and lasts 0.1 ms after the end of the chirp, for a total data capture duration of 186 ms to insure that all of the chirp signal is captured. The DSO has a maximum capture memory depth of 24 Msamples. The 186 ms data duration with 8 ns duration samples contains 23.25 Msamples, so there is a buffer of 750 Ksamples left empty in the capture memory. Of the 23.25 Msamples captured, there are 23.225 Msamples in the chirp duration of 185.8 ms.

The chirped amplitude modulated light output from the white light LED flashlight source illuminates the back wall of the light-tight box containing the source and a Hamamatsu H7828 Photon Counting Head, which has a stack of ND filters over its entrance aperture, which is pointed toward the illuminated spot on the back wall of the light-tight box.

The count pulses output by the photon counting head are input into the active data capture channel of the DSO, which samples the data at 125 Msps and stores the digital sample data in its local memory. This captured digital data is downloaded to a digital .csv file on a USB thumb drive plugged into the DSO. The USB thumb drive is removed from the DSO and plugged into a USB port on the mini-PC to transfer the captured digital data to the mini-PC for processing.

The count pulse output by the Hamamatsu H7828 photon counting head is 30 ns long. Since this is less than half of the 70 ns dead-time and more than 3 orders-of-magnitude shorter than the period of the highest frequency in the audio band (20 kHz frequency corresponding to 50 μs period), the count pulse is sufficiently short so that no edge-triggered pulse detector is needed in this experimental setup. In addition, the DSO's sample durations of 8 ns for the 125 Msps sampling rate, provide 3 samples across the 30 ns pulse. Thus, for each count pulse there will be 3 high level samples.

A segment of the raw count pulse data from the H7828's count pulse output captured by the DSO for the first proof-of-concept experiment for the bitstream PC-CAML with DLLO concept is shown in figure 15. The modulation of the count pulse density by the amplitude modulation of the transmitted signal is clearly seen in figure 15.

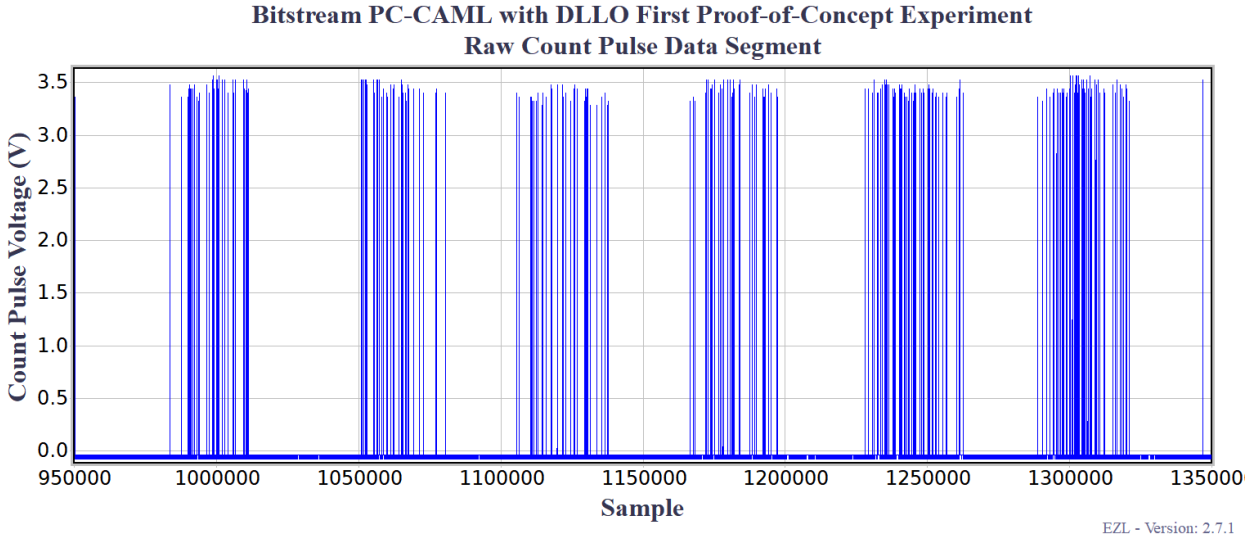

Figure 15. A segment of the raw count pulse data from the first proof-of-concept experiment for the bitstream PC-CAML with DLLO concept.

Since the H7828's count pulse high level is 3.0 to 3.5 V, positive logic and the digital data from the DSO is multi-bit data not single-bit binary data, the first step in the data processing is to convert the multi-bit data to single-bit binary data (i.e., 0 or 1) by setting all sample values above 0.3 V to 1 and all other sample values to zero.

In order to get the LO data at the correct 125 Msps sampling rate, a .wav file of the chirped square wave digital data at 192 Ksps sampling rate was created and streamed to the Oppo player, which output the line level analog waveform for the chirped square wave LO, which was input into the DSO to sample the LO waveform at 125 Msps with the same settings as used for collecting the photon counting data. That multi-bit digital LO data was binarized to signed binary data to produce the bipolar digital logic LO. Creating the LO in this way had the advantage of having exactly the same record length and trigger delays from the o-scope for both the signal and LO data, so the signal and LO data samples were automatically aligned.

Since the mixing with the LO is done digitally, the single set of counts digital data captured in the experiment can be processed with a DLLO that is a single-bit unipolar chirped square wave or a single signed bit chirped bipolar square wave with or without I/Q demodulation by generating each type of DLLO and saving it to a digital data file to be read in as needed for digitally mixing with the counts digital data captured in the experiment. Since it is no more difficult to generate and use the signed single-bit chirped bipolar square wave DLLO than the single-bit chirped unipolar DLLO, one may as well use the bipolar DLLO for the improved SNR. Thus, a unipolar DLLO was not generated. Only bipolar DLLOs were generated and used.

Figure 16 shows the Power Spectral Density (PSD) of the chirped unipolar sinusoidal modulation proof-of-concept experiment data processed with single-bit mixing with the signed single-bit bipolar DLLO without using I/Q demodulation, annotated with the experimental SNR in dB result measured from this PSD and the SNR in dB calculated using the SNR theory presented in section 2 for comparison. The theoretical and experimental SNRs differ by 0.1 dB.

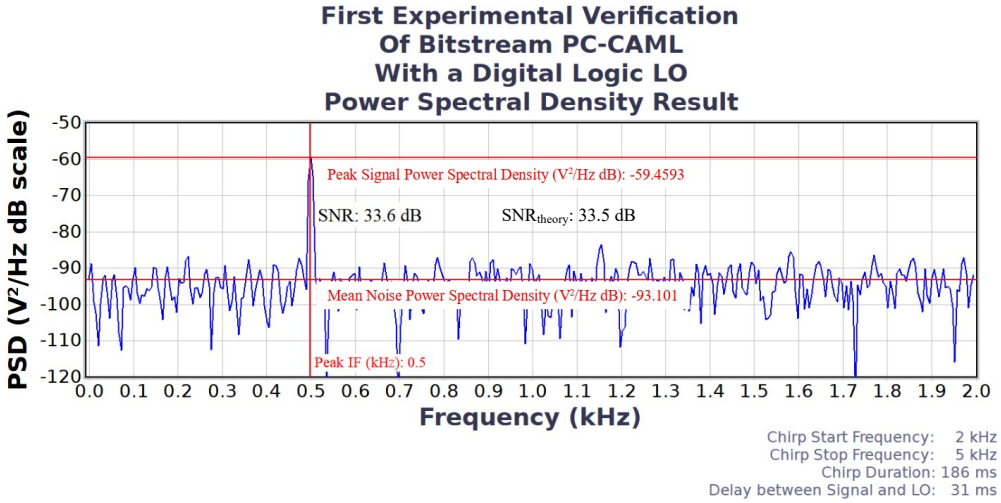

Figure 16. Proof-of-Concept Experimental Result: Power Spectral Density (PSD) of the chirped unipolar sinusoidal modulation proof-of-concept experiment data processed with single-bit mixing with the signed single-bit bipolar DLLO without using I/Q demodulation.

Figure 17 shows the Power Spectral Density (PSD) of the chirped unipolar sinusoidal modulation proof-of-concept experiment data processed with single-bit mixing with the signed single-bit bipolar DLLO using digital I/Q demodulation, annotated with the experimental SNR in dB result measured from this PSD and the SNR in dB calculated using the SNR theory presented in section 2 for comparison. The theoretical and experimental SNRs differ by 0.06 dB.

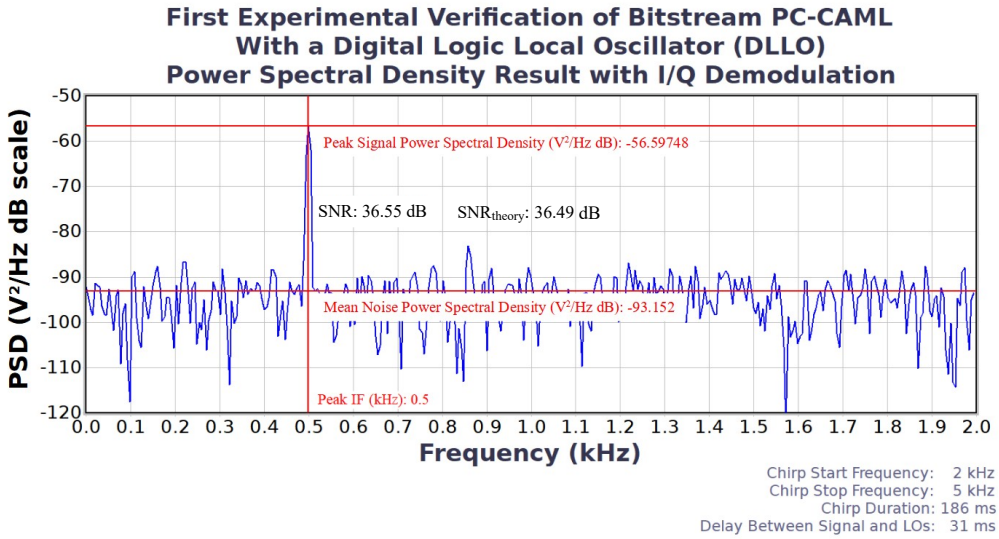

Figure 17. Proof-of-Concept Experimental Result: Power Spectral Density (PSD) of the chirped unipolar sinusoidal modulation proof-of-concept experiment data processed with single-bit mixing with the signed single-bit bipolar DLLO and using I/Q demodulation.

The following is a list of the values of the important parameters for the experiment and the theoretical calculations for the results shown in figures 16 and 17:

Parameters Common to Both No I/Q and With I/Q Demodulation:

fstart = 2000
fstop = 5000
B = 3000
dt = 4.8000e-04
Tchirp = 0.1858
Tnoise = 0.1860
Ns = 387.08
Fsamp = 1.2500e+08
tsamp = 8.0000e-09
Nsamples = 2.3225e+07
t_dead = 7.0000e-08
Counts_noise_meas = 15
Counts_noise_meas_rate = 80.643
PE_noise_Tnoise = 15.000
PE_noise_rate = 80.644
PE_noise = 14.984
Counts_tot_meas = 38398
Counts_tot_meas_rate = 2.0666e+05
PE_tot = 3.8962e+04
PE_tot_rate = 2.0970e+05
PE_sig_avg = 3.8947e+04
PE_sig_avg_rate = 2.0962e+05
mu = 1
PE_sig_peak = 7.7893e+04
PE_sig_peak_rate = 4.1923e+05
ms = 100.62
mn = 0.038709
mt = 100.65
mq = 29.836
md = 0.014679
Alpha = 1.0146
PAss = 0.9857
eta_Hann = 0.6667
Mspkl = 1.0000e+08
Fsig = 4
FLO = 1

Parameters for No I/Q Demodulation:

FIQ = 2
Ftot = 8
eta_tot = 0.082143
SNR_theory = 2229.5
SNR_theory_dB = 33.482

Parameters for With I/Q Demodulation:

FIQ = 1
Ftot = 4
eta_tot = 0.1643
SNR_theory = 4459.0
SNR_theory_dB = 36.492

The experimental results and theoretical calculations for the SNR are in very good agreement, as expected for the low mean total counts per dead-time of 0.0145 for this data since this signal plus noise level is well below saturation. Note that since the source outputs incoherent broadband white light, it is expected that the signal should be Poissonian, so a high value for the diversity of 1E8 was assigned to M. Since for this data m_s is about 1E2, with M = 1E8, $m_s << M$ for this data, so that the statistics of the signal plus noise should be well approximated by the Poisson distribution and the random sampling should be alias-free.

6. Conclusion

The concept and initial performance modeling, simulation and proof-of concept experiment results for the new bitstream PC-CAML with a DLLO system were presented in this paper. The results of the initial SNR theory, Monte Carlo simulations and proof-of-concept experiment presented here indicate that the bitstream PC-CAML with a DLLO performs as expected for signal levels below those at the onset of receiver saturation. The agreement between the SNRs calculated from the theory and the SNRs calculated from the experimental data is very good.

At high signal levels nearing saturation, the SNRs for the simulation results for a unipolar chirped sinusoidal signal roll off due to the reduction in arm probability for the Gm-APD as the mean number of counts per dead-time approaches 1, i.e., at the onset of receiver saturation, in accordance with the SNR theory. Additional SNR reductions at high signal levels due to energy losses to higher order harmonics and to reductions in the apparent modulation depth of the received AM waveform, and SNR improvements as the signal level starts to saturate the receiver due to squaring off of some waveforms are not included in the initial SNR theory presented here, but may be inherent in the simulations. For a fully modulated chirped square wave signal and for the new dual unipolar chirped sinusoidal signal with wavelength tagging, at high levels near saturation, the SNR from the simulation results continues to increase as the mixer output approaches that for a deterministic chirped square wave signal, and the floor of the power spectrum of the mixer output becomes dominated by sidelobes and perhaps aliasing, depending on the signal bandwidth and sample rate.

At signals levels below the onset of saturation, the nonuniform additive random sampling provided by Geiger-mode detection of the random arrival times of the photons eliminates aliasing if the signal bandwidth, clock time interval, count pulse rise time, and number of accumulated signal photon counts meet the criteria given in sections 1.7 and 1.8. For signal levels above the onset of saturation where aliasing may occur, methods for removing or reducing aliasing developed for bitstream radars can be applied to bitstream PC-CAML, if necessary.

The issue of the higher order harmonics generated by the chirped square wave modulation can be mitigated by using the same methods for this used in bitstream radar. The effectiveness for bitstream PC-CAML with a DLLO of one of these methods, that of applying an additional delay on the transmitted waveform to move the harmonics to frequencies higher than the intermediate frequency of the desired unambiguous range, was demonstrated herein with simulation results.

The concept and initial performance modeling and simulation results for the dual unipolar signal with bipolar DLLOs and digital I/Q demodulation technique for the bitstream PC-CAML were

also presented here. The dual unipolar transmitted signal provides a bipolar signal for the PC-CAML receiver, which was previously thought to be impossible. For the simulation results presented here, the dual unipolar chirped sinusoidal signal with bipolar DLLOs and digital I/Q demodulation compared to the unipolar chirped sinusoidal signal with unipolar DLLOs without digital I/Q demodulation provides an improvement in SNR from about 9 dB to 12 dB, depending on M and the signal level, for signal levels up to a mean counts per dead-time of 0.5, which is before the start of receiver saturation, and up to about 45.5 dB improvement in maximum achievable SNR if the signal fully saturates the receiver, for both cases, or 18-20 dB maximum SNR improvement, depending on M, if the unipolar signal with unipolar DLLO and no I/Q demodulation configuration operates at its maximum SNR and the dual unipolar signal with unipolar DLLO and I/Q demodulation configuration operates fully saturated to achieve its maximum SNR. Keep in mind, however, that these SNR improvements come at the cost of increased transmitter and receiver complexity.

The key advantages of the bitstream PC-CAML with a DLLO are that it can be implemented in the unit cells of a photon counting lidar receiver's ROIC just by adding digital logic gates, and the received signal and LO consist of streams of single-bit or signed single-bit binary data, eliminating the need for bulky, power-hungry, and expensive wideband RF analog receiver electronics. The DLLO data can be computed prior to operation and stored in a buffer in each ROIC unit cell, or in a single buffer and distributed to each ROIC unit cell in real-time during operation. The DLLO data buffer can be a circular buffer for continuous repetition of the DLLO waveform digital data. Multi-GHz clocks and digital logic gates are readily implemented in inexpensive silicon CMOS ROICs, and Multi-tens-of-GHz can be attained with more expensive technologies. These advantages make the bitstream PC-CAML with a DLLO more suitable for compact lidar-on-a-chip systems and lidar array receivers than previous PC-CAML systems.

5. Suggestions for Future Work

Suggestions for future work include:

1. Develop an SNR theory and simulations that include aliasing, the harmonics and their mixing products, apparent signal modulation depth reduction as the receiver saturates for some signal waveforms and apparent squaring off of other signal waveforms as the receiver saturates, the exact calculation of the arm probability for the signal waveform instead of using the approximate steady-state arm probability, timing errors and synchronization errors between dual unipolar signal channels.
2. Perform lab experiments at different signal levels up to and including receiver saturation for both the unipolar signal and the dual unipolar signal with wavelength tagging, and compare the results with the SNR theory.
3. Determine if negative binomial plus Poisson (NBPP) distributed random sampling is alias-free for all spectra for any sampling duration like Poisson point sampling, and if not, determine the minimum number of counts for alias-free sampling for this ARS process.
4. For bitstream PC-CAML, investigate detection at a harmonic frequency as used for improved range resolution in bitstream radar.
5. Investigate methods for suppressing harmonics and sidelobes for bitstream PC-CAML.

6. Investigate eliminating the power-hungry RF electronics for modulating the transmitted beam in the bitstream PC-CAML transmitter by using, for example, very low power photonic integrated circuit (PIC) laser sources that can be directly modulated at low voltage and current or followed with low voltage and current PIC waveguide modulators, the modulated output of which is amplified by semiconductor optical amplifiers (SOAs) or optical fiber amplifiers. [ref 31]
7. Build and test breadboard and brassboard bitstream PC-CAML with a DLLO prototypes.

6. Acknowledgments

The author thanks Philip Gatt of Lockheed Martin Coherent Technologies (LMCT) and Barry Stann of the United States Army Research Laboratory (ARL) for their helpful discussions and suggestions. The work reported herein was funded and executed solely by the author.

7. References:

1. Patent US7675610B2, "Photon counting, chirped AM LADAR system and related methods," Inventors: Brian Redman, William C. Ruff, and Barry L. Stann, Assignee: US Secretary of Army. Available at https://patents.google.com/patent/US7675610B2/en .

2. Brian Redman, William Ruff, and Mark Giza, "Photon counting chirped AM ladar: concept, simulation, and initial experimental results," Proc. SPIE 6214, Laser Radar Technology and Applications XI, 62140P, 19 May 2006.

3. Brian Redman, William Ruff, and Mark Giza, "Photon Counting Chirped AM Ladar: Concept, Simulation, and Experimental Results," 25th Army Science Conference, AP-14, November, 2006. Available at https://apps.dtic.mil/dtic/tr/fulltext/u2/a481357.pdf

4. B. Redman, W. Ruff, and M. Giza, "Photon Counting Chirped AM Ladar: Concept and Simulation Results," Conference on Lasers and Electro-Optics/Quantum Electronics and Laser Science Conference and Photonic Applications Systems Technologies, Technical Digest, paper PthA4, 2006.

5. Brian C. Redman and Barry L. Stann, "Photon Counting Chirped Amplitude Modulation Ladar," Army Research Laboratory Technical Report, ARL-TN-305, March, 2008. Available at the link: https://www.arl.army.mil/arlreports/2008/ARL-TN-305.pdf .

6. Zijing Zhang, Long Wu, Yong Zhang, and Yuan Zhao, "Method to improve the signal-to-noise ratio of photon-counting chirped amplitude modulation ladar," Appl. Opt. 52, pp. 274-279, 2013.

7. Zijing Zhang, Yuan Zhao, Yong Zhang, Long Wu, and Jianzhong Su, "Improvement of range accuracy of photon counting chirped AM ladar using phase postprocessing," Appl. Opt. 52, pp. 2447-2453, 2013.

8. Zijing Zhang, Jianlong Zhang, Long Wu, Yong Zhang, Yuan Zhao, and Jianzhong Su, "Photon-counting chirped amplitude modulation lidar using a smart premixing method," Opt. Lett. 38, pp. 4389-4392, 2013.

9. Zhaohui Li, Zeyu Bao, Yafan Shi, Baicheng Feng, E. Wu, Guang Wu, and Heping Zeng, "Photon-Counting Chirped Amplitude Modulation Lidar With 1.5-GHz Gated InGaAs/InP APD," IEEE Photonics Technology Letters, vol. 27, no. 6, pp. 616-619, March 15, 2015.

10. Zijing Zhang, Longzhu Cen, Jiandong Zhang, Kun Ma, Feng Wang, and Yuan Zhao, "Photon counting chirped amplitude modulation lidar using an asymmetric triangular wave modulation," Proc. SPIE 10141, Selected Papers of the Chinese Society for Optical Engineering Conferences held July 2016, 101410V, 7 November 2016.

11. Zijing Zhang, Long Wu, and Yuan Zhao, "Premixing photon-counting chirped amplitude modulation lidar for range and velocity measurement in photon starved scenes," Optik, Volume 127, Issue 24, pp. 11800-11806, December 2016. Available at the following link: https://kundoc.com/pdf-premixing-photon-counting-chirped-amplitude-modulation-lidar-for-range-and-veloc.html (click on the PDF Reader tab to view/download the paper).

12. Yi-Fei Sun, Zi-Jing Zhang, Li-Yuan Zhao, Wei-Min Sun, and Yuan Zhao, "Detection performance improvement of photon counting chirped amplitude modulation lidar with response probability correction," Chinese Physics B, Volume 27, Number 9, 2018. Available at the link: http://cpb.iphy.ac.cn/article/2018/1953/cpb_27_9_094213.html .

13. Zhou Hui, He Yu-Hao, Lü Chao-Lin, You Li-Xing, Li Zhao-Hui, Wu Guang, Zhang Wei-Jun, Zhang Lu, Liu Xiao-Yu, Yang Xiao-Yan, and Wang Zhen, "Photon-counting chirped amplitude modulation lidar system using superconducting nanowire single-photon detector at 1550-nm wavelength," Chinese Physics B, 27(1): 018501, 2018. Available at the link: http://cpb.iphy.ac.cn/article/2018/1919/cpb_27_1_018501.html .

14. Zijing Zhang, Long Wu, Yu Zhang, Yuan Zhao, and Xiudong Sun, "Detection performance improvement of chirped amplitude modulation ladar based on Gieger-mode [sic] avalanche photoelectric detector," Applied Optics, Vol. 50, No. 35, pp. 6522-6525, 10 December 2011.

15. Øystein Bjørndal, Svein-Erik Hamran, and Tor Sverre Lande, "UWB waveform generator for digital CMOS radar," 2015 IEEE International Symposium on Circuits and Systems (ISCAS), pp. 1510–1513, 2015.

16. Øystein Bjørndal, Svein-Erik Hamran, and Tor Sverre Lande, "Square wave architectures for radar-on-chip," 46th European Microwave Conference (EuMC), pp. 1485–1488, 2016.

17. Øystein Bjørndal, Svein-Erik Hamran, and Tor Sverre Lande, "Bitstream radar waveforms for generic single-chip-radar," International Journal of Microwave and Wireless Technologies, 9(6):1325–1337, August 2017.

18. Øystein Bjørndal, "Single Bit Radar Systems for Digital Integration," Department of Informatics, University of Oslo (UiO) & Norwegian Defence Research Establishment (FFI), September 2013 – September 2017, Ph.D Thesis, 2017. Available at the following link: https://www.duo.uio.no/handle/10852/59510 (also contains references 15-17).

19. Shanshan Shen, Qian Chen, Weiji He, Chen Yunfei, Yin Wenye, and Huidong Dai, "Research on Performance of Random Bitstream Ranging System Based on Single Photon Detection Theory [J]," Acta Optica Sinica, 2014, 34(10): 1012001. Available at http://www.opticsjournal.net/Articles/Abstract/gxxb/34/10/1012001.cshtml

20. Shanshan Shen, Qian Chen, Weiji He, and Huidong Dai, "Theory research on performance of high-speed random bitstream ranging system based on single-photon counting," Proc. SPIE 9279, Real-time Photonic Measurements, Data Management, and Processing, 92790Y (13 November 2014). Available at the following link: https://www.researchgate.net/publication/289576917_Theory_research_on_performance_of_high-speed_random_bitstream_ranging_system_based_on_single-photon_counting .

21. Kashif Siddiq, Mervyn K. Hobden, Robert J. Watson, Steve R. Pennock, and Steve Martins, "On phase measurement in FMCW Radar Systems," 7th Conference of the Sensor Signal Processing for Defence, SSPD 2017, London, UK, 6/12/17, vol. 2017-January, IEEE, pp. 1-4. https://doi.org/10.1109/SSPD.2017.8233250 . Also available at https://purehost.bath.ac.uk/ws/portalfiles/portal/183130666/On_phase_measurement_in_FMCW_Radar_Systems.pdf .

22. Shaofeng Shu, "Oversampling Digital-to-Analog Converters," Thesis, Oregon State University, completed June 7, 1995. Available at the following link: https://ir.library.oregonstate.edu/downloads/sq87bx73v .

23. F. J. Beutler, "Alias free randomly timed sampling of stochastic processes," IEEE Trans. Information Theory IT-16, pp. 147-152, March, 1970. Available at the following link: https://deepblue.lib.umich.edu/bitstream/handle/2027.42/3574/bab1190.0001.001.pdf?sequence=5&isAllowed=y .

24. King Chuen Lo, "Theory and realization of novel algorithms for random sampling in digital signal processing," Durham theses, Durham University, Available at Durham E-Theses Online: http://etheses.dur.ac.uk/5239/ , 1996.

25. Chenchi Luo, "Non-uniform Sampling: Algorithms and Architectures," Thesis, Georgia Institute of Technology, December, 2012. Available at the following link: https://smartech.gatech.edu/bitstream/handle/1853/45873/luo_chenchi_201212_phd.pdf .

26. Philip Gatt, Steven Johnson, and Terry Nichols, "Geiger-mode avalanche photodiode ladar receiver performance characteristics and detection statistics," Applied Optics, Vol. 48, No. 17, pp. 3261-3276, 10 June 2009.

27. https://en.wikipedia.org/wiki/Negative_binomial_distribution#Gamma%E2%80%93Poisson_mixture

28. John D. Cook, "Notes on the Negative Binomial Distribution," Available at the following link: https://www.johndcook.com/negative_binomial.pdf , October 28, 2009.

29. Axel Klein, "Logic Operators on Delta-Sigma Bit-Streams," Math. Comput. Appl. 2018, 23(1), 4. Available at the following link: https://doi.org/10.3390/mca23010004 .

30. H.E. Jones, "An Adaptive Digital Voice Multiplexer Using Walsh Functions," in Applications of Walsh Functions 1972 Proceedings, R.W. Zeek and A.E. Showalter, Editors, Symposium Held 27-29 March 1972, p. 112.

31. Christophe Kopp, Segolene Olivier, and Stephane Bernabe, CEA-LETI, EuroPhotonics, Spring 2017, see the discussion of PIC laser sources and modulators after figure 4 at https://www.photonics.com/Articles/Silicon_Photonics_Light_Is_the_Ultimate_Medium/a61635 .